



# Dark matter in the CP-violating NMSSM

Waqas Ahmed, Mark Goodsell, Shoaib Munir

## ► To cite this version:

Waqas Ahmed, Mark Goodsell, Shoaib Munir. Dark matter in the CP-violating NMSSM. European Physical Journal C: Particles and Fields, 2022, 82 (6), pp.539. 10.1140/epjc/s10052-022-10449-z . hal-03559935

**HAL Id: hal-03559935**

**<https://hal.science/hal-03559935>**

Submitted on 6 Feb 2024

**HAL** is a multi-disciplinary open access archive for the deposit and dissemination of scientific research documents, whether they are published or not. The documents may come from teaching and research institutions in France or abroad, or from public or private research centers.

L'archive ouverte pluridisciplinaire **HAL**, est destinée au dépôt et à la diffusion de documents scientifiques de niveau recherche, publiés ou non, émanant des établissements d'enseignement et de recherche français ou étrangers, des laboratoires publics ou privés.



# Dark matter in the CP-violating NMSSM

Waqas Ahmed<sup>1,a</sup>, Mark Goodsell<sup>2,b</sup>, Shoaib Munir<sup>3,c</sup> 

<sup>1</sup> School of Mathematics and Physics, Hubei Polytechnic University, Huangshi 435003, China

<sup>2</sup> Laboratoire de Physique Théorique et Hautes Energies (LPTHE), UMR 7589, Sorbonne Université et CNRS, 4 place Jussieu, 75252 Paris Cedex 05, France

<sup>3</sup> East African Institute for Fundamental Research (ICTP-EAIFR), University of Rwanda, Kigali, Rwanda

Received: 30 January 2022 / Accepted: 18 May 2022 / Published online: 18 June 2022  
© The Author(s) 2022

**Abstract** In the Next-to-Minimal Supersymmetric Standard Model there is a strong correlation between the mass terms corresponding to the singlet Higgs and the singlino interaction states, both of which are proportional to the parameter  $\kappa$ . If this parameter is complex, explicit CP-violation occurs in the Higgs as well as the neutralino sectors of the model at the tree level, unlike in the minimal scenario. A small magnitude of  $\kappa$  typically yields a  $\mathcal{O}(10)$  GeV lightest neutralino with a dominant singlino component. In such a scenario, the phase of  $\kappa$ , beside modifying the properties of the five Higgs bosons, can also have a crucial impact on the phenomenology of the neutralino dark matter. In this study we perform a first investigation of this impact on the relic abundance of the dark matter solutions with sub-100 GeV masses, obtained for parameter space configurations of the model that are consistent with a variety of current experimental data.

## 1 Introduction

Supersymmetric (SUSY) models with unbroken  $R$ -parity provide a viable candidate for the dark matter (DM) of the Universe, in the form of their lightest neutralino. The neutralinos are the mass eigenstates resulting from the mixing of the neutral fermionic superpartners of the electroweak (EW) gauge and Higgs bosons, and have Majorana masses. In the minimal supersymmetric Standard Model (MSSM) [1, 2], which contains two complex Higgs super-multiplets, there are four neutralinos,  $\tilde{\chi}_{1,2,3,4}^0$ . The interaction strengths of these neutralinos with Standard Model (SM) and SUSY particles are governed by their masses and compositions, i.e., the sizes of their *bino*, *wino* and *higgsino* components.

The two scalar Higgs doublet fields of the MSSM yield a total of five Higgs states. In the limiting case when all the parameters in the Higgs and sfermion sectors are real, these states include two neutral scalars  $h$  and  $H$  (with  $m_h < m_H$ ), a pseudoscalar  $A$ , and a charged pair  $H^\pm$ . In any model of new physics, (at least) one neutral scalar, which we generically refer to as the  $H_{\text{SM}}$  here, ought to have properties consistent with those of the  $H_{\text{obs}}$  discovered at the Large Hadron Collider (LHC) [3–5], i.e., a mass near 125 GeV and SM-like coupling strengths. In the MSSM, maximising the tree-level mass of the lighter scalar  $h$ , which has an upper limit equal to the  $Z$  boson mass, pushes the model into the so-called decoupling limit, where additionally its couplings to the vector bosons mimic those of the  $H_{\text{obs}}$ . Still, in order for  $m_h$  to reach  $\sim 125$  GeV, large loop corrections are needed from mainly the top quark, and its superpartners, the stops [6, 7]. As for the  $\tilde{\chi}_1^0$ , its consistency with the Planck measurement of the DM relic abundance of the Universe,  $\Omega_h^2$ , for a mass below about 1 TeV is only possible if it has a substantial bino component [8–13].

The Next-to-MSSM (NMSSM) [14–17] (see, e.g., [18, 19] for reviews) is obtained by adding a Higgs singlet superfield in the MSSM, which results in raising the upper limit on the tree-level mass of the  $H_{\text{SM}}$  in the model. This reduces the dependence of the  $H_{\text{SM}}$  mass on the stop sector, and hence alleviates the fine-tuning problem to some extent. Due to the presence of the extra singlet superfield, the neutral Higgs sector of the NMSSM contains three scalars,  $H_{1,2,3}$ , and two pseudoscalars,  $A_{1,2}$ . Crucially, in the NMSSM there exists the possibility of the next-to-lightest CP-even Higgs boson,  $H_2$ , acting as the  $H_{\text{SM}}$ , with the lighter, sometimes even considerably so,  $H_1$  still remaining undetected at the Large Electron Positron (LEP) collider as well as the LHC.

The neutralino sector of the NMSSM also contains a fifth state which, when the lightest of all, can differ significantly from the  $\tilde{\chi}_1^0$  of the MSSM in its properties. In particular,

<sup>a</sup> e-mail: waqasmit@hbpu.edu.cn

<sup>b</sup> e-mail: goodsell@lpthe.jussieu.fr

<sup>c</sup> e-mail: smunir@eaifr.org (corresponding author)

in the above-mentioned scenario with the SM-like  $H_2$ , the  $\tilde{\chi}_1^0$  typically has a large singlino component, and a mass  $\mathcal{O}(10)\text{ GeV}$  or even lower. Since the  $H_1$ , and generally also the  $A_1$ , lie below  $\sim 100\text{ GeV}$  [20, 21], this opens up multiple self-annihilation channels for the  $\tilde{\chi}_1^0$ , which are precluded in the MSSM, in order to generate the correct  $\Omega_h^2$  [22–27]. Potential LHC signatures of such a DM have been studied in [28–42], and its detection prospects in [43–45] (see also [46] for a phenomenological study of the DM in a two-Higgs doublet model with an additional singlet scalar).

Besides providing one of the leading candidates for low-mass DM, the NMSSM also entertains the possibility of explicit CP-violation in its Higgs sector at the tree level. This could serve as the additional source of CP-violation required for explaining the observed matter-antimatter asymmetry in the Universe through EW baryogenesis [47–51]. In the SM, the Cabibbo–Kobayashi–Maskawa (CKM) matrix is the lone and insufficient source of CP-violation, while the MSSM Higgs sector can only violate CP at higher orders [52–63]. The CP-violating phases of the SUSY-breaking Higgs-fermion-fermion couplings,  $A_{\tilde{f}}$ , where  $f$  denotes a SM fermion, in the MSSM can be radiatively transmitted to the Higgs sector, but are tightly constrained by the measurements of fermion electric dipole moments (EDMs) [64, 65]. In the NMSSM, if the Higgs self-couplings,  $\lambda$  and/or  $\kappa$ , appearing in the superpotential are complex, the scalar and pseudoscalar interaction eigenstates mix together to give five neutral CP-indefinite Higgs states; see [66–71] for recent studies of the NMSSM Higgs sector with CP violation and [72] for a review. We henceforth refer to this model as the cNMSSM.

Several phenomenological scenarios emerging in the cNMSSM Higgs sector that are distinct from the NMSSM with real parameters (rNMSSM) have been studied in [73–78]. Importantly, the complex  $\kappa$  parameter associated with the singlet superfield also appears in the entry of the neutralino mass matrix that corresponds to the singlino weak eigenstate. The impact of a non-zero phase of  $\kappa$  on the phenomenology of the  $\tilde{\chi}_1^0$  DM has not been analysed in literature thus far. In this article, we take a first step in this direction, and investigate how the relic abundance of the  $\tilde{\chi}_1^0$  in the cNMSSM is affected by variations in this phase. We focus mainly on the (EW-scale) cNMSSM parameter space configurations that yield a sub-100 GeV DM, which can be predominantly singlino-like. We also test the consistency of these solutions with the most important latest experimental constraints, including the Higgs boson data from the LHC and the electron and neutron EDMs, and study some of their phenomenological implications.

The article is organised as follows. In the next section we briefly revisit the Higgs and neutralino sectors of the cNMSSM. Section 3 contains details of our numerical analysis of the model's parameter space with the focus on the DM

observables. In Sect. 4 we present the results of our analysis, and we summarise our findings in Sect. 5.

## 2 The NMSSM with explicit CP-violation

### 2.1 The Higgs sector

The superpotential of the NMSSM is written as

$$W_{\text{NMSSM}} = \hat{U}^C \mathbf{h}_u \hat{Q} \hat{H}_u + \hat{D}^C \mathbf{h}_d \hat{Q} \hat{H}_d + \hat{E}^C \mathbf{h}_e \hat{H}_d \hat{L} + \mu \hat{H}_u \hat{H}_d + \lambda \hat{S} \hat{H}_u \hat{H}_d + \frac{\kappa}{3} \hat{S}^3 \quad (1)$$

in terms of the singlet Higgs superfield,  $\hat{S}$ , besides the two  $SU(2)_L$  doublet superfields,

$$\hat{H}_u = \begin{pmatrix} \hat{H}_u^+ \\ \hat{H}_u^0 \end{pmatrix}, \quad \hat{H}_d = \begin{pmatrix} \hat{H}_d^0 \\ \hat{H}_d^- \end{pmatrix}, \quad (2)$$

of the MSSM. The above superpotential observes a discrete  $Z_3$  symmetry, which is imposed in order to explicitly break the dangerous  $U(1)_{PQ}$  symmetry, and renders it conformal-invariant by forbidding the  $\mu \hat{H}_u \hat{H}_d$  term present in the MSSM superpotential. Here, the mixing between the  $H_d^0$  field and the  $H_u^0$  fields, necessary for each of them having a non-trivial vacuum expectation value (TeV) at the minimum of the potential, is instead generated by the  $\lambda \hat{S} \hat{H}_u \hat{H}_d$  term. This results in a dynamic  $\mu_{\text{eff}} \equiv \lambda s / \sqrt{2}$  term when the singlet field acquires a VEV,  $s$ , naturally near the SUSY-breaking scale.

The tree-level Higgs potential of the NMSSM is obtained as

$$V_0 = \left| \lambda \left( H_u^+ H_d^- - H_u^0 H_d^0 \right) + \kappa S^2 \right|^2 + \left( m_{H_u}^2 + |\lambda S|^2 \right) \left( \left| H_u^0 \right|^2 + \left| H_u^+ \right|^2 \right) + \left( m_{H_d}^2 + |\lambda S|^2 \right) \left( \left| H_d^0 \right|^2 + \left| H_d^- \right|^2 \right) + \frac{g_1^2 + g_2^2}{8} \left( \left| H_u^0 \right|^2 + \left| H_u^+ \right|^2 - \left| H_d^0 \right|^2 - \left| H_d^- \right|^2 \right)^2 + \frac{g_2^2}{2} \left| H_u^+ H_d^{0*} + H_u^0 H_d^{-*} \right|^2 + m_S^2 |S|^2 + \left( T_\lambda \left( H_u^+ H_d^- - H_u^0 H_d^0 \right) S + \frac{1}{3} T_\kappa S^3 + \text{h.c.} \right), \quad (3)$$

where  $g_1$  and  $g_2$  are the  $U(1)_Y$  and  $SU(2)_L$  gauge couplings. It is customary to define the trilinears proportional to the superpotential couplings as

$$T_\lambda \equiv \lambda A_\lambda, \quad T_\kappa \equiv \kappa A_\kappa. \quad (4)$$

$A_\lambda$  and  $A_\kappa$  above are the soft SUSY-breaking counterparts of the superpotential couplings, and all of these can very well be complex parameters, with the corresponding phases,  $e^{i\phi_{A_\lambda}}$ ,  $e^{i\phi_{A_\kappa}}$ ,  $e^{i\phi_\lambda}$ , and  $e^{i\phi_\kappa}$ .

After spontaneous EW symmetry breaking,  $V_0$  is evaluated at the vacuum, in terms of fields defined around their respective VEVs,  $v_u$ ,  $v_d$  and  $s$ , as

$$\begin{aligned} H_d^0 &= \begin{pmatrix} \frac{1}{\sqrt{2}}(v_d + H_{dR} + iH_{dI}) \\ H_d^- \end{pmatrix}, \\ H_u^0 &= e^{i\theta} \begin{pmatrix} H_u^+ \\ \frac{1}{\sqrt{2}}(v_u + H_{uR} + iH_{uI}) \end{pmatrix}, \\ S &= \frac{e^{i\varphi}}{\sqrt{2}}(s + S_R + iS_I). \end{aligned} \quad (5)$$

The potential then contains the phase combinations

$$\begin{aligned} \phi'_\lambda - \phi'_\kappa \text{ (with } \phi'_\lambda \equiv \phi_\lambda + \theta + \varphi \text{ and } \phi'_\kappa \equiv \phi_\kappa + 3\varphi), \\ \phi'_\lambda + \phi_{A_\lambda}, \text{ and } \phi'_\kappa + \phi_{A_\kappa}. \end{aligned}$$

However, assuming vanishing spontaneous phases  $\theta$  and  $\varphi$ , the last two phase combinations above can be determined up to a twofold ambiguity using the minimisation conditions of  $V_0$ , leaving  $\phi'_\lambda - \phi'_\kappa$  as the only physical CP phase (see [75] for more details).

The potential  $V_0$  with complex phases leads to a  $5 \times 5$  Higgs mass matrix,  $\mathcal{M}_0^2$ , in the  $\mathbf{H}^T = (H_{dR}, H_{uR}, S_R, H_I, S_I)$  basis, with the massless Nambu–Goldstone mode rotated away. After including the higher order corrections from various sectors of the model [73, 75, 79], the resulting Higgs mass matrix,  $\mathcal{M}_H^2 = \mathcal{M}_0^2 + \Delta\mathcal{M}^2$ , is diagonalised using an orthogonal matrix,  $O$ , as  $O^T \mathcal{M}_0^2 O = \text{diag}(m_{H_1}^2, m_{H_2}^2, m_{H_3}^2, m_{H_4}^2, m_{H_5}^2)$ . The masses of the five CP-mixed physical Higgs bosons thus obtained are ordered such that  $m_{H_1}^2 \leq m_{H_2}^2 \leq m_{H_3}^2 \leq m_{H_4}^2 \leq m_{H_5}^2$ .

## 2.2 The Neutralino sector

As noted in the Introduction, the fermion component of  $\widehat{S}$ , called the singlino, mixes with the neutral gauginos,  $\widetilde{B}^0$  and  $\widetilde{W}_3^0$ , and higgsinos,  $\widetilde{H}_d^0$  and  $\widetilde{H}_u^0$ , to yield five neutralinos in the NMSSM. The symmetric neutralino mass matrix in the gauge eigenstate basis,  $\widetilde{\psi}^0 = (-i\widetilde{B}^0, -i\widetilde{W}_3^0, \widetilde{H}_d^0, \widetilde{H}_u^0, \widehat{S})$ , is written as

with  $m_W$  and  $\theta_W$  being the  $W$ -boson mass and the weak mixing angle, respectively. The neutralino masses and compositions at the tree level thus depend on the Higgs-sector parameters  $\lambda$ ,  $\kappa$ ,  $\mu_{\text{eff}}$ ,  $v_u$ ,  $v_d$  and the gaugino masses  $M_1$  and  $M_2$ . When any of these parameters is complex, the mass matrix in Eq. (6) can be diagonalised by a unitary matrix  $N$ , to give  $D = \text{diag}(m_{\widetilde{\chi}_i^0}) = N^* \mathcal{M}_{\widetilde{\chi}^0} N^\dagger$ , for  $i = 1 - 5$ . The neutralino mass eigenstates are then given by  $\widetilde{\chi}_i^0 = N_{ij} \widetilde{\psi}_j^0$ , and are again ordered as  $m_{\widetilde{\chi}_1^0} \leq m_{\widetilde{\chi}_2^0} \leq m_{\widetilde{\chi}_3^0} \leq m_{\widetilde{\chi}_4^0} \leq m_{\widetilde{\chi}_5^0}$ .

The  $\widetilde{\chi}_1^0$ , which is the lightest neutral SUSY particle and hence a DM candidate, is given by the linear combination

$$\widetilde{\chi}_1^0 = N_{11} \widetilde{B}^0 + N_{12} \widetilde{W}_3^0 + N_{13} \widetilde{H}_d^0 + N_{14} \widetilde{H}_u^0 + N_{15} \widehat{S}^0. \quad (7)$$

Thus, the relative sizes of the soft gaugino masses  $M_{1,2}$ , the  $\mu_{\text{eff}}$ -parameter and the  $\kappa s$  term determine whether the  $\widetilde{\chi}_1^0$  is gaugino-, higgsino- or singlino-like. For example, in the limit  $\mu_{\text{eff}} \ll \min[M_1, M_2]$ , the term  $[\mathcal{M}_{\widetilde{\chi}^0}]_{55} = 2\kappa s = 2\frac{\kappa\mu_{\text{eff}}}{\lambda}$  in Eq. (6) results in a singlino-dominated  $\widetilde{\chi}_1^0$  for  $2\kappa/\lambda < 1$ . Importantly, in SUSY models the charged higgsinos ( $\widetilde{H}_u^\pm$  and  $\widetilde{H}_d^\pm$ ) and winos ( $\widetilde{W}^\pm$  and  $\widetilde{W}^\pm$ ) also mix to form the chargino eigenstates,  $\widetilde{\chi}_a^\pm$  ( $a = 1, 2$ ). The mass matrix for the charginos is given by

$$\mathcal{M}_{\widetilde{\chi}^\pm} = \begin{pmatrix} M_2 & \sqrt{2}m_W \sin \beta \\ \sqrt{2}m_W \cos \beta & \mu_{\text{eff}} \end{pmatrix}. \quad (8)$$

This implies that  $M_2$  and  $\mu_{\text{eff}}$  have a lower bound of about 100 GeV, owing to the non-observation of a chargino at the LEP collider. Since no such constraint exists on the  $M_1$  and  $2\kappa s$  terms, the  $\widetilde{\chi}_1^0$  in the NMSSM can have a mass much lower than 100 GeV as long as it is predominantly bino- and/or singlino-like. The presence of a certain amount of higgsino is, however, necessary to obtain a realistic relic abundance.

The existence of the singlino in the NMSSM, even in the absence of the CP-violating phases noted above, leads to some unique possibilities in the context of DM phenomenology, compared to the MSSM. In the limit of large  $\tan \beta \equiv v_u/v_d$  and large  $m_A \equiv \frac{\lambda s}{\sin 2\beta}(\sqrt{2}A_\lambda + \kappa s)$  (which effectively decouples the doublet-like  $H_3$  and  $A_2$  from the rest of the particle spectrum, so that  $m_{A_2} \simeq m_A$ ), the masses of the two lightest CP-even scalars can be approximated by [80]

$$\mathcal{M}_{\widetilde{\chi}^0} = \begin{pmatrix} M_1 & 0 & -m_W \tan \theta_W \cos \beta & m_W \tan \theta_W \sin \beta & 0 \\ 0 & M_2 & m_W \cos \beta & -m_W \sin \beta & 0 \\ -m_W \tan \theta_W \cos \beta & m_W \cos \beta & 0 & -\mu_{\text{eff}} & -\lambda v_u \\ m_W \tan \theta_W \sin \beta & -m_W \sin \beta & -\mu_{\text{eff}} & 0 & -\lambda v_d \\ 0 & 0 & -\lambda v_u & -\lambda v_d & 2\kappa s \end{pmatrix}, \quad (6)$$

$$M_{H_1, H_2}^2 \approx \frac{1}{2} \left\{ m_Z^2 + 4(\kappa s)^2 + \kappa s A_\kappa \sqrt{[m_Z^2 - 4(\kappa s)^2 - \kappa s A_\kappa]^2 + 4\lambda^2 v^2 [2\lambda s - (A_\lambda + \kappa s) \sin 2\beta]^2} \right\}, \quad (9)$$

where  $v \equiv \sqrt{v_u^2 + v_d^2}$ . Thus the mass of the lighter of these two (when the heavier one is required to be the  $H_{SM}$ ) scales with  $\kappa s$ , as does that of the singlino. At the same time, the mass-squared of the lighter pseudoscalar, which is almost purely a singlet, reduces to

$$m_{A_1}^2 \simeq -3\kappa s A_\kappa. \quad (10)$$

This correlation between the masses of the  $A_1$  and the  $\tilde{\chi}_1^0$  implies that they can be naturally close to each other, thus opening the possibility of the former's self-annihilation via the latter. Evidently, while  $H_1$  can also have a mass in the vicinity of  $m_{A_1}$ , it is more strongly constrained by Eq. (9) from taking values close to  $2\tilde{\chi}_1^0$ . Even if it does acquire the correct mass, the  $\tilde{\chi}_1^0$  annihilation via  $s$ -channel  $H_1$  is  $p$ -wave suppressed, which would make its consistency with the thermal relic abundance difficult.

When the CP-violating phases of  $\kappa$  and  $\lambda$  are turned on, they enter the tree-level neutralino mass matrix independently of each other, unlike the combination  $\phi'_\lambda - \phi'_\kappa$  of the Higgs sector. In addition,  $M_1$  and  $M_2$  can also be complex parameters, which would be radiatively induced into the Higgs sector at higher orders. Given the composition of the  $\tilde{\chi}_1^0$ , the size(s) of the most relevant phase(s) would then affect not only its physical mass, but also its interaction strengths with other particles. Here, our focus on a sub-100 GeV DM, which is also preferably singlino-like (since low-mass bino-like solutions exist in the MSSM too and have been extensively studied), makes  $\phi_\kappa$  the most obvious choice to investigate the impact of.

### 2.3 The electric dipole moments of fermions

Beyond the Born approximation, various CP-violating phases are (co-)induced in the Higgs and neutralino sectors of the cNMSSM. Such phases are subject to constraints from the non-observation of the EDMs of the electron and the neutron. The most recent limits on these EDMs read

$$|d_e| < 1.1 \times 10^{-29} e \text{ cm} [81]; \quad |d_n| < 1.8 \times 10^{-26} e \text{ cm} [82]. \quad (11)$$

The limit on the electron EDM above is based on the thorium monoxide experiment, and is more stringent than the one from the HfF<sup>+</sup> experiment [83]. In SUSY models, the one-loop EDMs of the charged leptons and the light quarks are induced by chargino and neutralino exchange diagrams.

These should in principle constrain the CP-violating phases of  $M_1$ ,  $M_2$ ,  $\lambda$  and  $\kappa$ , appearing in the chargino/neutralino sectors at the tree level. In the SUSY spectrum generator code used for our analysis, details of which will be provided in the next section, calculation of the one-loop contributions to  $d_e$  and  $d_n$ , as well as to  $d_\tau$ , in the cNMSSM is currently implemented. Note that additional constraints also come from mercury [84] and thallium [85] EDMs, but these can generally be evaded if the masses of the first two generations of squarks are taken to be sufficiently heavy, as discussed in [66].

At the two-loop level, the Higgs-mediated Barr-Zee type diagrams can also contribute significantly to the electron and neutron EDMs. However, several studies have shown that even when these two-loop effects are taken into account, the phase  $\phi'_\kappa$  is very weakly constrained by the fermionic EDMs [73, 76, 86, 87], especially for smaller values of  $|\kappa|$ . This is in contrast with the other phases, especially  $\phi_{A_{\tilde{f}}}$  (the phases of the Higgs-sfermion-sfermion trilinear couplings), which enter the Higgs sector at the one-loop level. Therefore, besides the reason noted above, we choose the  $\phi'_\kappa$  as the sole representative CP-violating phase additionally to minimise the potential impact of these two-loop diagrams, which are not accounted for in our numerical code. Implementation of the complete set of contributions to the EDMs in our numerical code would go beyond the scope of this article, which aims to explore the DM properties when a non-zero phase appears in the neutralino sector.

## 3 Numerical analysis

The radiative corrections to the tree-level Higgs and neutralino mass matrices make the parameters of the other model sectors highly relevant also. However, on the one hand, the NMSSM with grand-unification-inspired boundary conditions is very tightly constrained by the current experimental results, and on the other hand, the most general NMSSM contains more than a hundred free parameters defined at the EW scale. Thus, in order to draw inferences for a particular sector of the model, it is imperative to make multiple assumptions about the free parameters that only impinge at higher orders.

For our numerical analysis, we therefore adopted the following (universality) conditions to impose on the parameter space of the  $Z_3$ -symmetric cNMSSM at the EW scale:

$$M_{\tilde{f}} \equiv M_{Q_{1,2,3}} = M_{U_{1,2,3}} = M_{D_{1,2,3}} = M_{L_{1,2,3}} = M_{E_{1,2,3}}, \\ T_{\tilde{f}} \equiv T_{\tilde{t}} = T_{\tilde{b}} = T_{\tilde{\tau}},$$



where  $M_{Q_{1,2,3}}^2$ ,  $M_{U_{1,2,3}}^2$ ,  $M_{D_{1,2,3}}^2$ ,  $M_{L_{1,2,3}}^2$  and  $M_{E_{1,2,3}}^2$  are the squared soft masses of the sfermions. The (less-often used) parameter  $T_{\tilde{f}}$  corresponds to sfermion trilinear couplings; usually these are taken to be proportional to the Yukawas, such that  $T_{\tilde{f}}^{ij} = Y_u^{ij} A_{\tilde{f}}$ , where  $i, j$  are generation indices. In our numerical code, we specified  $T_{\tilde{f}}$  directly at the low scale. We fixed all the elements of  $T_{\tilde{f}}$  to small values (1 GeV for the diagonal terms and zero otherwise), except for  $T_{\tilde{f}}^{(3,3)} = T_{\tilde{t}}^{(3,3)} = T_{\tilde{b}}^{(3,3)} = T_{\tilde{\tau}}^{(3,3)}$ , which we left as a free parameter to be scanned over an extended range. The reason for this was to increase the probability of the consistency of  $m_{H_{SM}}$ , the dominant corrections to which increase proportionally to  $(A_{\tilde{f}} - \mu_{\text{eff}} \cot \beta)^2$ , with  $m_{H_{\text{obs}}}$ . We likewise scanned over wide ranges of  $M_1$  and  $M_2$  to allow maximal possible variations in the  $\tilde{\chi}_1^0$  composition. On the other hand,  $M_{\tilde{f}}$  and  $M_3$  were fixed to sufficiently large values of 2 TeV and 3 TeV, respectively, so that the sfermions and the gluino could evade the direct search limits from the LHC.

As for the CP-violating phases, in light of the discussion in the previous section, we fixed  $\phi'_\lambda = \phi_{M_1} = \phi_{M_2} = \phi_{T_{\tilde{f}}} = \varphi = \theta = 0$  (so that  $\phi'_\kappa = \phi_\kappa$ ). However, the quantities that we choose for the solution of the (five independent) tadpole equations are

$$m_{H_d}^2, m_{H_u}^2, m_S^2, \text{Im}(T_\kappa), \text{Im}(T_\lambda).$$

The first three of these are standard choices familiar from the rNMSSM. However, once we break CP we have two additional non-trivial tadpole equations that must be satisfied, and it is logical to choose the complex part of the trilinear parameters, since these lead to the smallest impact on the spectrum and their magnitude will only be proportional to the violation of CP. With the only non-zero CP-violating phase being  $\phi_\kappa$ , this leads to

$$\begin{aligned} \text{Im}(T_\lambda) &= \mu_{\text{eff}} \text{Im}(\kappa) - \frac{\sqrt{2}}{sv_u} \text{Re} \left( \frac{\partial \Delta V_0}{\partial H_{dI}} \right), \\ \text{Im}(T_\kappa) &= \frac{3\lambda v_d v_u}{\sqrt{2}s} \text{Im}(\kappa) + \frac{\sqrt{2}}{s^3} \text{Re} \left( s \frac{\partial \Delta V_0}{\partial S_I} - v_d \frac{\partial \Delta V_0}{\partial H_{dI}} \right). \end{aligned} \quad (12)$$

As briefly noted in Sect. 2.1, the real parts of these trilinears are fixed as inputs:

$$\begin{aligned} \text{Re}(T_\lambda) &= \text{Re}(\lambda A_\lambda), \\ \text{Re}(T_\kappa) &= \text{Re}(\kappa A_\kappa), \end{aligned} \quad (13)$$

where now  $A_\lambda, A_\kappa$  are taken to be real. This means that at the tree level both the trilinear couplings pick up phases from the phase of  $\kappa$  (which are, however, small for  $A_\lambda \gg \mu_{\text{eff}}$  and  $A_\kappa \gg v_d v_u/s$ , and are modified at the higher orders).

To generate the particle spectrum for a given configuration of the final set of the free parameters,

$$|M_1|, |M_2|, |T_{\tilde{f}}|, \tan \beta, |\lambda|, |\kappa|, \mu_{\text{eff}}, A_\lambda, A_\kappa, \phi_\kappa,$$

we incorporated the cNMSSM into the public fortran code SPheno-v4.0.4 [88,89] using the Mathematica package SARAH-v4.14.4 [66,90–95].<sup>1</sup> Besides the mass spectrum, SPheno also computes the decay widths and branching ratios (BRs) of the Higgs and SUSY particles (at one loop for CP-conserving models [97], but at leading order only for CP-violating ones), as well as a multitude of flavour and other low-energy observables. We linked SPheno with the public program MultiNest-v3.7 [98] for generating output files for sampled configurations of the free parameters from their defined ranges. Multiple scans were performed, with each one corresponding to  $\phi_\kappa$  fixed to one of the five selected values:  $0^\circ$  (the CP-conserving case, i.e., the rNMSSM but with the five Higgs bosons ordered by their masses, irrespective of their CP-identities),  $30^\circ$ ,  $60^\circ$ ,  $135^\circ$ , and  $180^\circ$ .<sup>2</sup> In order to calculate  $\Omega_{\tilde{\chi}_1^0} h^2$  and other DM observables for each sampled parameter space point, we also produced a CalcHEP [99] model file for the cNMSSM with SARAH, which was then embedded in the public code MicrOmegas-v5.2.4 [100–102].

The purpose of these scans was to find parameter space points for which

1. Either  $H_2$  or  $H_3$  had a mass in the 122–128 GeV range (thus allowing a theoretical uncertainty of  $\pm 3$  GeV around the - assumed - experimental central value of  $m_{H_{SM}} = 125$  GeV). This implied that there would at least be one light Higgs boson available for potential  $s$ -channel annihilation of the DM.
2. The  $H_{SM}$  (whether  $H_2$  or  $H_3$ ) had the  $\gamma\gamma$ ,  $ZZ$ ,  $\tau\tau$  and  $b\bar{b}$  effective couplings lying within  $\pm 0.2$  units of the SM expectation of 1.<sup>3</sup>

<sup>1</sup> We note that NMSSMTools provides a spectrum generator capable of handling CP violation [79] that contains a less accurate computation of the Higgs masses; whereas NMSSMCALC [96] provides an equivalent computation of the Higgs masses [71].

<sup>2</sup> We ignored  $\phi_\kappa > \pi$ , since we expected the real part of  $\kappa$  to be dominant by far, and hence the overall behaviors of the calculated observables to be approximately symmetric around  $\phi_\kappa = \pi$ . This was nevertheless verified numerically for the sample value of  $\phi_\kappa = 300^\circ$ .

<sup>3</sup> While it is in principle possible to constrain these couplings using the latest combined measurements from the LHC (e.g., [103]) using a program like HiggsSignals-2 [104] instead we chose (for simplicity) to allow up to 20% deviation from the SM values. The figure of 20% corresponds roughly to the experimentally quoted uncertainties (we also checked that using a smaller value negligibly impacted our results); we were concerned that a combination was overly pessimistic regarding finding valid points, and not primarily concerned with tweaking the (heavier)  $H_{SM}$  which otherwise plays little role in the dark matter properties.

**Table 1** Scanned ranges of the cNMSSM parameters. Separate scans were run for  $\phi_\kappa$  chosen from  $\{0^\circ, 30^\circ, 60^\circ, 135^\circ, 180^\circ\}$ 

Parameter Range	$M_1$ (GeV) [1, 1000]	$M_2$ (GeV) [100, 2000]	$T_{\tilde{f}}$ (GeV) [− 7000, − 2000]	$\tan \beta$ [1, 20]	
Parameter Range	$\lambda$ [0.1, 0.7]	$\kappa$ [0.001, 0.3]	$\mu_{\text{eff}}$ (GeV) [100, 500]	$A_\lambda$ (GeV) [500, 3000]	$A_\kappa$ (GeV) [ $\mp 500, 0$ ]

3. The theoretical predictions of the following  $B$ -physics observables lied within  $2\sigma$  deviation from their quoted experimental values.

- $\text{BR}(B \rightarrow X_s \gamma) \times 10^4 = 3.32 \pm 0.15$  [105],
- $\text{BR}(B_u \rightarrow \tau^\pm \nu_\tau) \times 10^4 = 1.06 \pm 0.19$  [105],
- $\text{BR}(B_s \rightarrow \mu^+ \mu^-) \times 10^9 = 3.0 \pm 0.85$  [106].

4. None of the five Higgs states were excluded by the limits from the LEP, TeVatron and LHC searches implemented within the program HiggsBounds-v5.7.0 [107].

5. The  $|d_e|$  and  $|d_n|$  satisfied the experimental upper bounds given in Eq. (11).

6. The relic abundance of the  $\tilde{\chi}_1^0$  never exceeds +10% of the Planck measurement of  $\Omega h^2 = 0.119$  [108]. This allowance in  $\Omega_{\tilde{\chi}_1^0} h^2$  is to crudely account for the rather large uncertainty in its theoretical estimation, due to the higher order corrections in SUSY models [109–115]. Note that MultiNest performs a multimodal sampling of a model's parameter space based on Bayesian evidence estimation. Our purpose for using this package was simply to scan the parameter space in a more efficient way than random sampling, rather than to draw Bayesian inferences about it. To this end, we defined a Gaussian likelihood function with a peak at  $\Omega_{\tilde{\chi}_1^0} h^2 = 0.119$  and a width of  $\pm 10\%$  of this value in MultiNest. Evidently, the scan collected a number of points far away from the peak also. From these, we removed all the points with  $\Omega_{\tilde{\chi}_1^0} h^2 > 0.131$ , but retained also the ones for which  $\Omega_{\tilde{\chi}_1^0} h^2 < 0.107$  so as to accommodate alternative possibilities, such as non-thermal  $\tilde{\chi}_1^0$  production [116] or multi-component DM [117].

#### 4 Low-mass DM in the cNMSSM

The scanned ranges of the nine free parameters (after fixing  $\phi_\kappa$ ) of the cNMSSM are given in Table 1. Evidently, these ranges cannot entail all possible configurations. They are, however, guided by some previous studies [20, 33, 35], and are extensive enough to fulfill the necessary conditions for this analysis, i.e., of yielding a  $H_2$  or  $H_3$  with a mass around 125 GeV, and a sub-100 GeV singlino/bino-dominated  $\tilde{\chi}_1^0$ . The upper cutoffs on the values of  $\lambda$  and  $\kappa$  are imposed to

**Table 2** The input parameters and the spectra for the four selected test points

Parameter	TP1	TP2	TP3	TP4
$M_1$ (GeV)	42	386	689	602
$M_2$ (GeV)	1967	1565	1273	773
$T_{\tilde{f}}$ (GeV)	− 2688	− 3414	− 3938	− 4132
$\tan \beta$	13.69	10.80	14.82	6.84
$\lambda$	0.227	0.323	0.659	0.252
$ \kappa $	0.178	0.012	0.003	0.016
$\mu_{\text{eff}}$	458	252	192	322
$A_\lambda$ (GeV)	2694	2613	2904	2165
$A_\kappa$	− 11.70	− 2.44	− 57.45	− 31.06
Parameter	TP1	TP2	TP3	TP4
$\phi_\kappa$ (degrees)	30	30	30	30
$\Omega h^2$	0.130	0.127	0.119	0.079
$m_{\tilde{\chi}_1^0}$ (GeV)	41	20	6	43
$m_{\tilde{\chi}_2^0}$ (GeV)	463	251	216	317
$m_{\tilde{\chi}_3^0}$ (GeV)	469	265	228	333
$m_{\tilde{\chi}_4^0}$ (GeV)	723	393	688	603
$m_{\tilde{\chi}_5^0}$ (GeV)	1973	1578	1292	804
$m_{\tilde{\chi}_1^\pm}$ (GeV)	466	256	193	323
$m_{\tilde{\chi}_2^\pm}$ (GeV)	1988	1597	1310	813
$m_{h_1}$ (GeV)	87	16	14	45
$m_{h_2}$ (GeV)	125	45	69	52
$m_{h_3}$ (GeV)	720	124	127	123
$m_{h_4}$ (GeV)	4302	2671	2970	2196
$m_{h_5}$ (GeV)	4302	2672	2974	2196
$m_{H^\pm}$ (GeV)	4303	2651	2830	2188

avoid the Landau pole.  $A_0$  can in principle be both positive and negative, with a marginally different impact on the physical mass of the SM-like Higgs boson for an identical set of other input parameters in each case. Our purpose for using only its negative range was to enhance the efficiency of the numerical scanning code. Note that, at the EW scale  $\kappa$  and  $A_\kappa$  are conventionally taken to be  $> 0$  and  $< 0$ , respectively, in order to prevent negative mass-squared of the lightest pseudoscalar – see Eq. (10). But here, for  $90^\circ < \phi_\kappa < 180^\circ$ , the real part of  $\kappa$  becomes negative, and hence  $A_\kappa$  ought to be positive. Thus in the scans corresponding to  $\phi_\kappa = 135^\circ$  and  $180^\circ$ ,  $A_\kappa$  was scanned over positive values only.

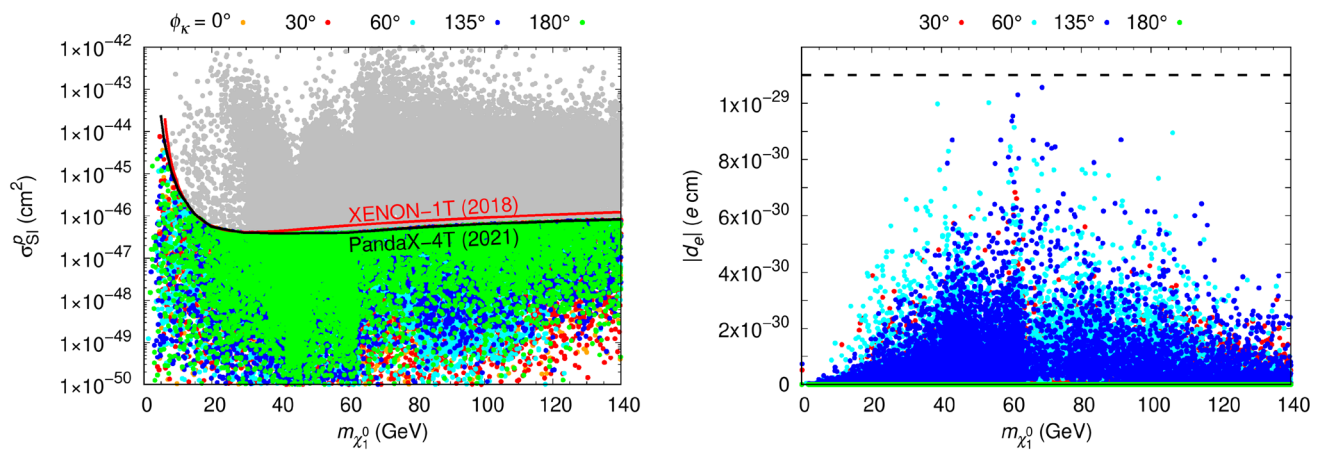


**Fig. 1** The spin-independent DM-proton cross section (left) and the electron EDM (right) as functions of the DM mass. Different colours of the points illustrate different values of  $\phi_\kappa$ , and the solid and dashed lines in the left and right panels, respectively, correspond to the experimental limits

The left panel of Fig. 1 shows that a large number of parameter space points meeting all the conditions outlined in the previous section are ruled out by the latest limits on the cross section of the spin-independent DM-proton scattering,  $\sigma_{SI}^p$ , from the PandaX-4T Commissioning Run [118] (for comparison, the most recent exclusion contour from the XENON-1T experiment [119] is also shown). The right panel confirms the fact that  $\phi_\kappa$  is indeed very weakly constrained by the one-loop contributions to  $|d_e|$ , since for almost all the successful scanned points its model prediction lies well below the experimental bound.

In Fig. 2 the  $\tilde{\chi}_1^0$  relic abundance is plotted as a function of its mass, separately for points from each scan with fixed  $\phi_\kappa$ . In this figure, the grey points in the background are the ones excluded by the PandaX-4T limits, and the coloured points further satisfy the following two conditions.

- The total invisible BR of the  $H_{SM}$  is required to lie below the latest upper limit of 14.5% from ATLAS [120] (the corresponding limit from CMS [121] is slightly weaker). This BR accounted for, besides  $H_{SM} \rightarrow \tilde{\chi}_1^0 \tilde{\chi}_1^0$ , decays like  $H_{SM} \rightarrow \tilde{\chi}_i^0 \tilde{\chi}_1^0$  ( $i = 2-5$ ), which are followed by  $\tilde{\chi}_i^0 \rightarrow H_1 \tilde{\chi}_1^0 / H_2 \tilde{\chi}_1^0$  and subsequently  $H_1 / H_2 \rightarrow \tilde{\chi}_1^0 \tilde{\chi}_1^0$ . In addition, BRs for  $H_{SM} \rightarrow H_1 H_1 / H_1 H_2 / H_2 H_2$ , followed by  $H_1 / H_2 \rightarrow \tilde{\chi}_1^0 \tilde{\chi}_1^0$ , which would also yield a  $4\tilde{\chi}_1^0$  final state, were also included. For all the good points from our scans, however, the total invisible BR of  $H_{SM}$  is by far dominated by the  $\tilde{\chi}_1^0 \tilde{\chi}_1^0$  decay.
- Various searches targeting  $\tilde{\chi}_1^\pm$  and  $\tilde{\chi}_i^\pm$  production, such as [122–124], are relevant here, since these states can decay to our (very) light  $\tilde{\chi}_1^0$  along with  $W/Z/H_{obs}$ . These analyses quote limits of up to 750 GeV for winos with specific channels of decay. Searches for higgsinos are notoriously difficult due to their small production cross-section, and the limits from them are thus much weaker. The very

latest ATLAS search [125] quotes limits of up to 210 GeV on a higgsino. A full recasting of these results using MadAnalysis [131–134] for all our good points will go beyond the scope of this study. We nevertheless imposed the simplistic requirement that the higgsino (wino) component of a given  $\tilde{\chi}_i^0$  is less than 90% if it is lighter than 210 GeV (750 GeV).

In the top-left panel of the Fig. 2, corresponding to the CP-conserving case,  $\Omega_{\tilde{\chi}_1^0} h^2$  is generally quite small, except near  $m_{\tilde{\chi}_1^0} \sim m_Z/2$  and  $m_{\tilde{\chi}_1^0} \sim m_{H_{SM}}/2$  for the  $H_{SM} = H_3$  scenario (blue points), where a few points show consistency with the Planck measurement within  $\pm 10\%$ . A narrow peak of points also appears around  $m_{\tilde{\chi}_1^0} \sim 10$  GeV, where, as we will see later, a very singlino-like  $\tilde{\chi}_1^0$  can undergo just the right amount of self-annihilation via the singlet  $A_1$ . Recall that all the five Higgs bosons are ordered by mass and not distinguished by their CP-assignment, and thus the  $H_1$  in the cNMSSM can be either one of the  $H_1$  or  $A_1$  of the rNMSSM. In the  $H_{SM} = H_2$  scenario (red points) the correct  $\Omega_{\tilde{\chi}_1^0} h^2$  can be obtained for a wide range of  $m_{\tilde{\chi}_1^0}$ , when it is near either  $m_{H_2}/2$  or, more frequently,  $m_{H_3}/2$ . For  $\phi_\kappa = 30^\circ$ , in the top-right panel, a few points with  $m_{\tilde{\chi}_1^0}$  between 10–20 GeV also appear within (or just outside) the Planck band (i.e.,  $\Omega h^2 = 0.119 \pm 10\%$ ). This is not the case for the CP-conserving case above, although the overall picture looks very similar, and is a result of the slight modification in the  $\tilde{\chi}_1^0$  composition owing to the CP-violating phase.

When  $\phi_\kappa$  is increased to  $60^\circ$  (centre-left panel) some Planck-consistent points show up also around  $m_{\tilde{\chi}_1^0} = 30$  GeV. Most notably, however, it is possible to obtain the correct  $\Omega_{\tilde{\chi}_1^0} h^2$  for the entire  $\sim 5-40$  GeV mass range when the sign of  $\kappa$  (and hence also of  $A_\kappa$ ) is flipped, as demonstrated by the centre-right and bottom-left panels corresponding to  $\phi_\kappa = 135^\circ$  and  $\phi_\kappa = 180^\circ$ , respectively. In fact, for the



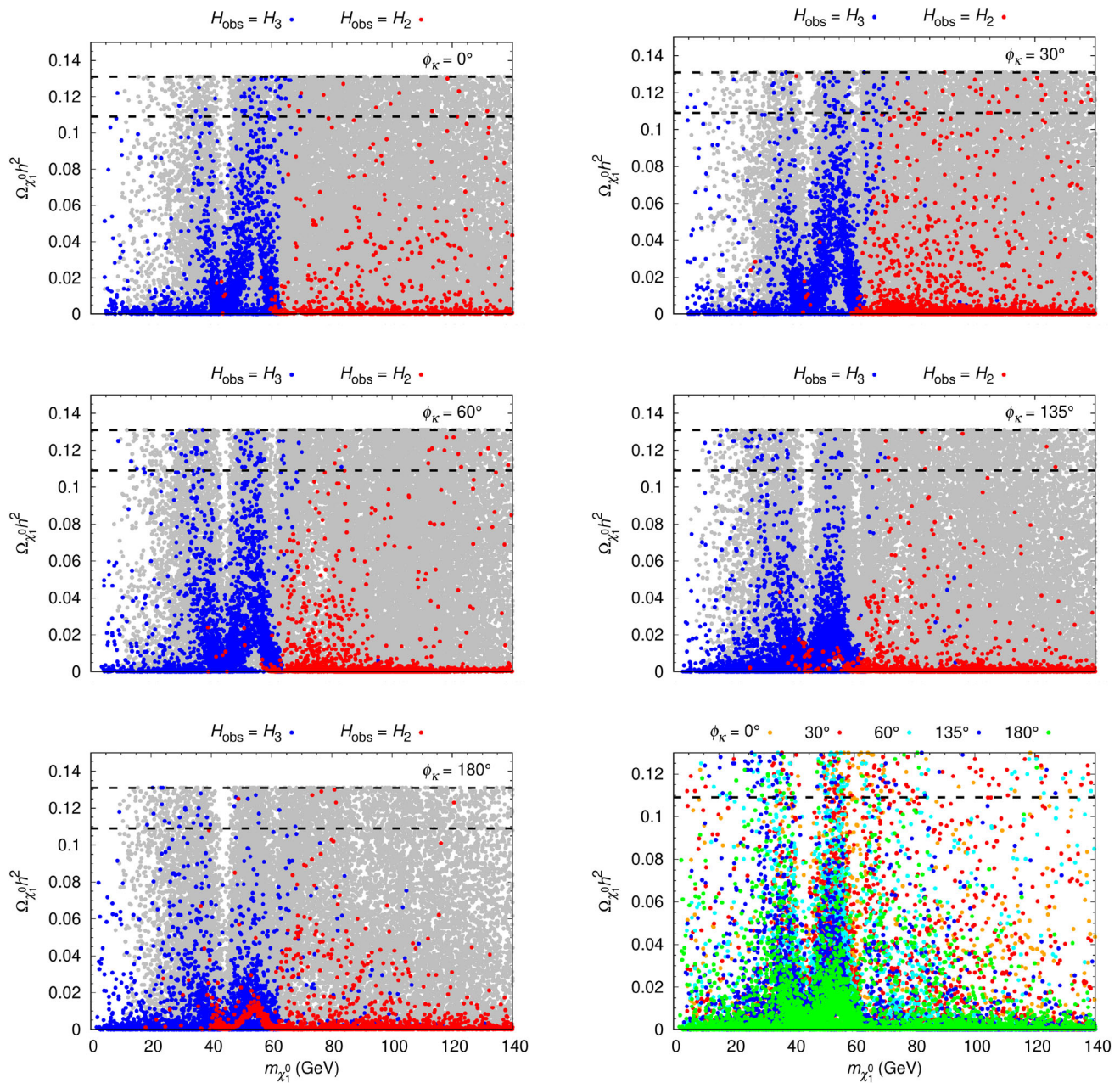


**Fig. 2** Relic abundance of the DM as a function of its mass, for points obtained from the scans with  $\phi_K$  fixed to  $0^\circ$  (top-left),  $30^\circ$  (top-right),  $60^\circ$  (centre-left),  $135^\circ$  (centre-right), and  $180^\circ$  (bottom-left). The red points correspond to the  $H_{\text{SM}} = H_2$  scenario and the blue points to the

latter phase, a sole point appears within the Planck band for  $m_{\tilde{\chi}_1^0}$  in the  $\sim 40$ – $45$  GeV range (which is, however, excluded by the LHC electroweakino searches). This is not observed for any of the other selected phases in this figure, but we will discuss below a point for which it is achieved around  $\phi_K = 60^\circ$  also. The bottom-right panel presents a holistic picture, where one sees that nearly the entire sub-100 GeV range of  $m_{\tilde{\chi}_1^0}$  with  $\Omega h^2 = 0.119 \pm 10\%$  is covered by the good points from all of the scans.

$H_{\text{SM}} = H_3$  one. The grey points in the background are the ones ruled out by the PandaX-4T limits on  $\sigma_{\text{SI}}^p$ . The bottom-right panel shows the allowed points from all the other panels overlapped

For a closer analysis of the impact of the variation in  $\phi_K$  on  $m_{\tilde{\chi}_1^0}$  and its relic abundance, we selected four test points (TPs) from among those corresponding to  $\phi_K = 30^\circ$ . The values of the corresponding scanned parameters, along with the spectra for  $\phi_K = 30^\circ$ , are given in Table 2. For each of these TPs,  $m_{\tilde{\chi}_1^0}$  is plotted as a function of  $\phi_K$  in all the panels of Fig. 3. The heat map in the left column of the figure corresponds to  $m_{H_1}$  and in the right column to  $m_{H_2}$ . In this as well as the two figures that follow, the non-existence of a point for some

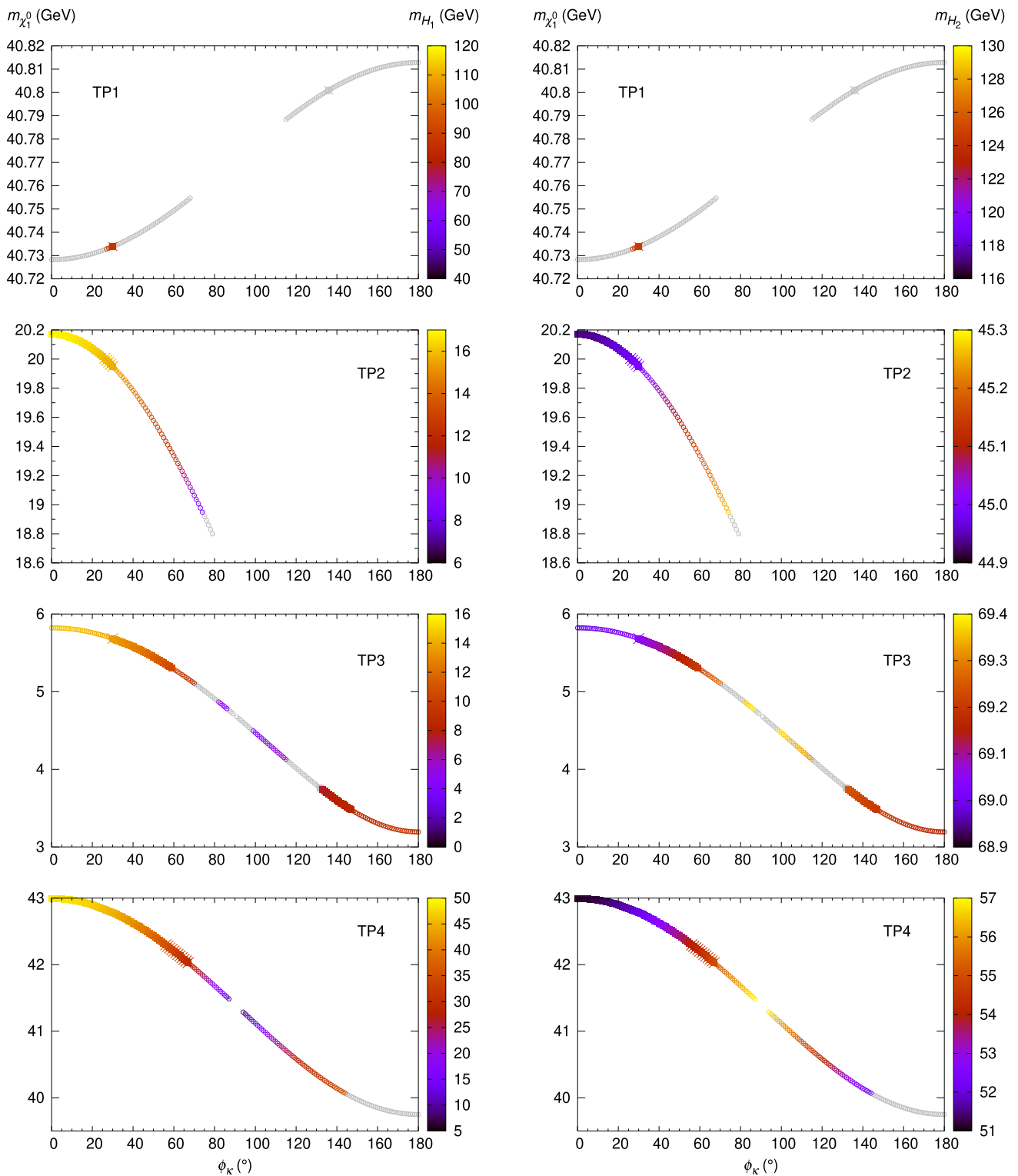


**Fig. 3**  $m_{\tilde{\chi}_1^0}$  as a function of  $\phi_\kappa$  for the test points 1 (top row)–4 (bottom row). The heat maps correspond to  $m_{H_1}$  (left column),  $m_{H_2}$  (right column). The grey circles imply inconsistency with one of the experimental constraints, while the coloured circles give  $\Omega_{\tilde{\chi}_1^0} h^2 > 0.131$ .

The coloured boxes correspond to  $\Omega_{\tilde{\chi}_1^0} h^2 < 0.131$ , and a cross around a box implies  $0.107 < \Omega_{\tilde{\chi}_1^0} h^2 < 0.131$ , besides consistency with all the other constraints

values of  $\phi_\kappa$  in a given panel implies that *SPheno* did not produce an output on account of there being unphysical loop-corrected masses for some particles. The grey points imply inconsistency with one (or more) of the constraints 1–5 listed in Sect. 3 and the two additional limits from the LHC noted above, while the coloured circles give  $\Omega_{\tilde{\chi}_1^0} h^2 > 0.131$ . The coloured boxes instead mean  $\Omega_{\tilde{\chi}_1^0} h^2 < 0.131$  for that point, and a cross around a box reflects that  $\Omega_{\tilde{\chi}_1^0} h^2$  lies within the Planck band.

The TP1 in the top row of Fig. 3 is the single (red) point for the  $H_{SM} = H_2$  scenario with  $m_{\tilde{\chi}_1^0} \sim 40$  GeV appearing within the Planck band for  $\phi_\kappa = 30^\circ$ . It does so, however, only for this specific value of  $\phi_\kappa$ . For almost the entire remaining range of the phase, this parameter space configuration is inconsistent with at least one of the enforced experimental constraints. The remaining three TPs belong to the  $H_{SM} = H_3$  scenario. For TP2 also, the Planck-consistent amount of self-annihilation of the  $\tilde{\chi}_1^0$ , via the  $H_2$ , occurs only for  $\phi_\kappa$  a few degrees around  $30^\circ$ .  $m_{\tilde{\chi}_1^0}$  and  $m_{H_2}$  both reduce with increasing  $\phi_\kappa$  – the latter much slower than the former – until tachyonic masses appear in the particle spectrum for  $\phi_\kappa \geq 80^\circ$ . In the case of TP3, as with the TP1,  $\Omega_{\tilde{\chi}_1^0} h^2 = 0.119 \pm 10\%$  is satisfied only for  $\phi_\kappa = 30^\circ$ , when the sharply falling  $m_{H_1}$  gets very close to  $2m_{\tilde{\chi}_1^0} \simeq 12$  GeV, as seen in the third row of the left panel. Beyond this value of  $\phi_\kappa$ , the  $\Omega_{\tilde{\chi}_1^0} h^2$  drops for a few degrees, owing to excessive annihilation, before rising above the Planck bound again when  $m_{H_1}$  grows too small. Finally, TP4 is a representative point of the case when the  $\Omega_{\tilde{\chi}_1^0} h^2$  falls within the Planck band for  $m_{\tilde{\chi}_1^0}$  in the  $\sim 40$ – $45$  GeV range, as hinted earlier. While this TP has also been taken from among the good points for  $\phi_\kappa = 30^\circ$  in Fig. 2, its  $\Omega_{\tilde{\chi}_1^0} h^2$  lies below the Planck band for the original  $\phi_\kappa$ .

In the left column of Fig. 4  $m_{\tilde{\chi}_1^0}$  is again plotted as a function of  $\phi_\kappa$  for the TPs 1–4 (top row to bottom row), with the heat map now depicting the singlino fraction,  $N_s$ , of the  $\tilde{\chi}_1^0$ . For TP1, the  $\tilde{\chi}_1^0$  has a negligible singlino component, but is instead entirely bino-like, with a small higgsino fraction just enough for the correct amount of its self-annihilation via the  $Z$  boson for  $\phi_\kappa = 30^\circ$ . On the other hand, the very large  $N_s$  in the CP-conserving case for TP2 falls sharply with increasing  $\phi_\kappa$ , with the Planck-consistency occurring when it is just above 90% around  $\phi_\kappa \sim 30^\circ$ . For TP3 the  $N_s$  stays almost constant over the entire range of  $\phi_\kappa$ , while for TP4, as the singlino fraction as well as the mass of  $\tilde{\chi}_1^0$  drop slowly with increasing  $\phi_\kappa$ , its  $Z$ -mediated annihilation gradually reduces. It reaches a level sufficient to give the correct  $\Omega_{\tilde{\chi}_1^0} h^2$  for  $\phi_\kappa \sim 55^\circ$ – $65^\circ$ . The right column of this figure shows the  $\text{BR}(H_{SM} \rightarrow \tilde{\chi}_1^0 \tilde{\chi}_1^0)$ . For TP1 it fluctuates between 1.5% and 2% for the allowed values of  $\phi_\kappa$ , and for TP2 it rises with  $\phi_\kappa$  but does not exceed 4%. For TP3 the  $\text{BR}(H_{SM} \rightarrow \tilde{\chi}_1^0 \tilde{\chi}_1^0)$  rises noticeably with  $\phi_\kappa$  (while  $m_{\tilde{\chi}_1^0}$ ,

given by the heat map, drops), until it reaches the maximum of about 10% for  $180^\circ$ , while for TP4 it is always insignificant.

In Fig. 5 we take a brief look at the BRs of the  $H_{SM}$  into  $H_1 H_1$  (left column) and  $H_2 H_2$  (right column), in a bid to further understand the implications of different  $\phi_\kappa$  for the  $H_{SM}$  phenomenology at the LHC. For TP1, the  $\text{BR}(H_2 \rightarrow H_1 H_1)$  is vanishing for the Planck-consistent  $\phi_\kappa = 30^\circ$ , while the  $H_3 \rightarrow H_2 H_2$  decay is kinematically forbidden. In the case of TP2, the  $\text{BR}(H_3 \rightarrow H_1 H_1)$  drops from about 12% in the CP-conserving case to about 8% for  $\phi_\kappa = 80^\circ$ , but the  $\text{BR}(H_{SM} \rightarrow H_2 H_2)$  increases by about 2%. The  $\text{BR}(H_3 \rightarrow H_1 H_1)$  for TP3 also falls by about 4% overall, as in the case of TP2. For TP4, the  $\text{BR}(H_3 \rightarrow H_1 H_1)$  drops from about 7% near  $\phi_\kappa = 0^\circ$  to less than 1% for  $\phi_\kappa = 180^\circ$ , implying that the already slim prospects of observing the 4-body final state resulting from  $H_{SM} \rightarrow H_1 H_1$  decay for this point further reduce significantly as the amount of CP-violation increases. At the same time, though, the  $\text{BR}(H_{SM} \rightarrow H_2 H_2)$  rises from  $\sim 6\%$  to about 17%, but this causes exclusion of  $\phi_\kappa > 144^\circ$  by the LHC data. Overall then, the phenomenology of the 4-body final states with invariant mass near that of  $H_{SM} = H_3$  for points analogous to the TP4 could be crucial for distinguishing the signatures of CP-conserving versus the CP-violating NMSSM. It will be the subject of a follow-up analysis.

Finally, since the  $\tilde{\chi}_1^\pm/\tilde{\chi}_2^0$  in all our TPs are higgsino-like and always heavier than 210 GeV, they are consistent with the current exclusion limits from the LHC. Besides, instead of decaying to  $W/Z/H_{\text{obs}}$ , our  $\tilde{\chi}_2^0$  can decay dominantly to the lighter singlet-like Higgs boson(s) and thus keep evading detection in the near future. Likewise, the  $\tilde{\chi}_2^\pm/\tilde{\chi}_3^0$  are wino-like and heavier than 750 GeV for these four points. Nevertheless, in our follow-up analysis it would be interesting to test our scan points against latest results using a fast tool such as *SModelS* [126–130], and to process a handful using full recasting in *MadAnalysis* with the latest searches in [135, 136] (see also [137] for a review of available recasting tools), as performed in, e.g., [138].

## 5 Summary and conclusions

The Higgs sector of the NMSSM can accommodate explicit CP-violating phases at the tree level, whereas in the MSSM such phases enter the Higgs potential only at the higher orders. While the measurements of the leptonic EDMs tightly bound the MSSM-like phase in  $A_{\tilde{f}}$ , radiatively induced from the sfermion sector, they have been previously found to be much less constraining of the phase of  $\kappa$ . Importantly, this phase also appears in the tree-level mass term,  $2\kappa s$ , corresponding to the singlino interaction eigenstate. Therefore, if the  $\tilde{\chi}_1^0$  is singlino-dominated, its relic abundance can have a strong dependence on  $\phi_\kappa$ .

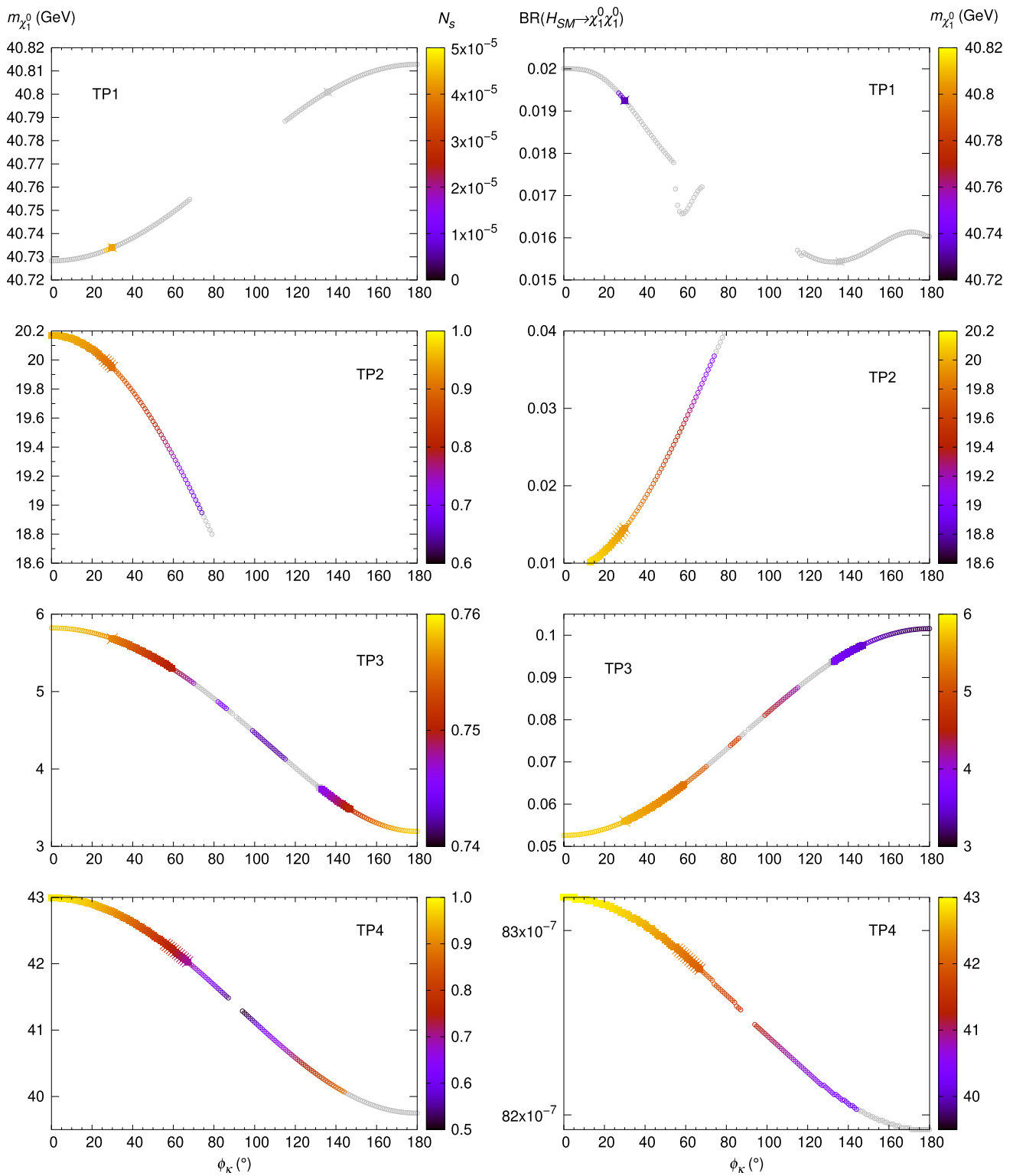


**Fig. 4**  $m_{\tilde{\chi}_1^0}$  (left column) and  $\text{BR}(H_{\text{SM}} \rightarrow \tilde{\chi}_1^0 \tilde{\chi}_1^0)$  (right column) as functions of  $\phi_\kappa$  for the test points 1 (top row)–4 (bottom row). The heat maps in the left and right columns correspond to  $N_s$  and  $m_{\tilde{\chi}_1^0}$ , respectively. The colouring scheme is the same as in Fig. 3

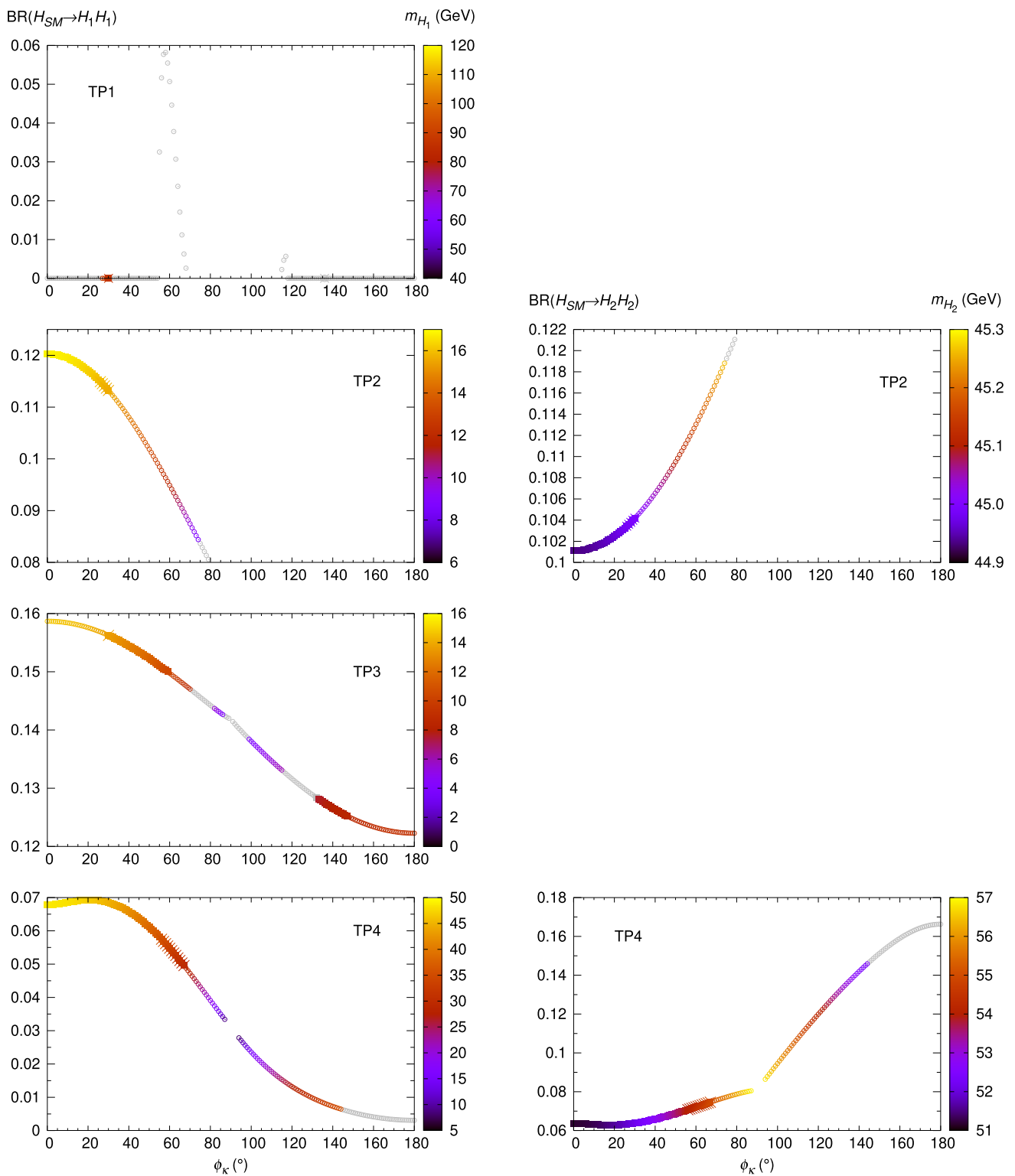


**Fig. 5**  $BR(H_{SM} \rightarrow H_1 H_1)$  (left column), (central column) and  $BR(H_{SM} \rightarrow H_2 H_2)$  (right column) as functions of  $\phi_k$  for the TPs 1 (top row)–4 (bottom row). The heat maps in the left and right columns correspond to  $m_{H_1}$  and  $m_{H_2}$ , respectively. The colouring scheme is the same as in Fig. 3



The cNMSSM contains 5 neutral CP-indefinite Higgs bosons in total, and any one (or more) of the three lightest of these can fulfil the role of the  $H_{\text{SM}}$ , in specific regions of the model's parameter space. In this study, we have analysed in detail the quantitative impact of the variation in  $\phi_\kappa$  on  $\Omega_{\tilde{\chi}_1^0} h^2$ , for scenarios wherein either  $H_{\text{SM}} = H_2$  or  $H_{\text{SM}} = H_3$ . The  $H_1$  was required to always be lighter than 125 GeV to increase the prospects of self-annihilation of the singlino-like  $\tilde{\chi}_1^0$  solutions with mass  $\lesssim 100$  GeV, which was our main focus. For certain select values of  $\phi_\kappa$ , we performed numerical scans of the free parameters of the EW-scale cNMSSM, to find points consistent with a variety of recent experimental constraints, in particular the electron EDM.

In the overall picture that emerges from this analysis, for specific values of  $\phi_\kappa$ , nearly exact consistency with the Planck measurement of the DM relic abundance of the Universe is seen for certain  $m_{\tilde{\chi}_1^0}$  that are precluded in the real NMSSM. Thus, while a large gap appears near  $\Omega_{\tilde{\chi}_1^0} h^2 0.119$  for  $m_{\tilde{\chi}_1^0} \sim 10\text{--}30$  GeV for  $\phi_\kappa = 0^\circ$ , this mass range starts filling up as the CP-violation increases, and gets almost entirely covered for  $\phi_\kappa \sim 135^\circ$ . Evidently, this results from the subtle tweaks in the composition of  $\tilde{\chi}_1^0$ , so that its couplings allow just the right amount of its self-annihilation via one of the multiple potentially resonant sources available in this model, when the CP is violated.

This inference was confirmed by a closer investigation of the four tests points selected out of the successful points from the scans. For each of these points we varied  $\phi_\kappa$  over the entire  $0^\circ - 180^\circ$ , while fixing the other nine free parameters to their original values. This demonstrated how the different values of  $\phi_\kappa$  modify  $m_{H_1}$  and  $m_{H_2}$ , besides the mass as well as the  $N_s$  of the  $\tilde{\chi}_1^0$ , to impact the consistency of these points not only with  $\Omega h^2$  but also with other experimental data. Furthermore, magnitudes of observables like the  $\text{BR}(H_{\text{SM}} \rightarrow \tilde{\chi}_1^0 \tilde{\chi}_1^0)$ , the  $\text{BR}(H_{\text{SM}} \rightarrow H_1 H_1)$  and the  $\text{BR}(H_{\text{SM}} \rightarrow H_2 H_2)$  also show a dependence on  $\phi_\kappa$  significant enough that their dedicated inspection might help identify signatures of CP-violation in the NMSSM at the LHC.

**Acknowledgements** The authors thank Shabbar Raza for his collaboration in the early stages of this project. MDG acknowledges support from the “HiggsAutomator” (ANR-15-CE31-0002) and “DMwithLL PatLHC” grants of the Agence Nationale de la Recherche (ANR).

**Data Availability Statement** This manuscript has no associated data or the data will not be deposited. [Authors' comment: The data can be easily reproduced using the public codes mentioned and the information provided in the text. It can also be shared with the reader upon request.]

**Open Access** This article is licensed under a Creative Commons Attribution 4.0 International License, which permits use, sharing, adaptation, distribution and reproduction in any medium or format, as long as you give appropriate credit to the original author(s) and the source, provide a link to the Creative Commons licence, and indicate if changes were made. The images or other third party material in this article are included in the article's Creative Commons licence, unless indi-

cated otherwise in a credit line to the material. If material is not included in the article's Creative Commons licence and your intended use is not permitted by statutory regulation or exceeds the permitted use, you will need to obtain permission directly from the copyright holder. To view a copy of this licence, visit <http://creativecommons.org/licenses/by/4.0/>.  
Funded by SCOAP<sup>3</sup>.

## References

1. H.P. Nilles, Supersymmetry, Supergravity and particle physics. Phys. Rep. **110**, 1–162 (1984)
2. H.E. Haber, G.L. Kane, The search for supersymmetry: probing physics beyond the standard model. Phys. Rep. **117**, 75–263 (1985)
3. ATLAS Collaboration, G. Aad et al., Observation of a new particle in the search for the Standard Model Higgs boson with the ATLAS detector at the LHC. Phys. Lett. B **716**, 1–29 (2012). [arXiv:1207.7214](https://arxiv.org/abs/1207.7214)
4. CMS Collaboration, S. Chatrchyan et al., Observation of a new boson at a mass of 125 GeV with the CMS experiment at the LHC. Phys. Lett. B **716**, 30–61 (2012). [arXiv:1207.7235](https://arxiv.org/abs/1207.7235)
5. CMS Collaboration, S. Chatrchyan et al., Observation of a new boson with mass near 125 GeV in pp collisions at  $\sqrt{s} = 7$  and 8 TeV. JHEP **1306**, 081 (2013). [arXiv:1303.4571](https://arxiv.org/abs/1303.4571)
6. A. Djouadi, The anatomy of electro-weak symmetry breaking. II. The Higgs bosons in the minimal supersymmetric model. Phys. Rep. **459**, 1–241 (2008). [arXiv:hep-ph/0503173](https://arxiv.org/abs/hep-ph/0503173)
7. M. van Beekveld, S. Caron, R. Ruiz de Austri, The current status of fine-tuning in supersymmetry. JHEP **01**, 147 (2020). [arXiv:1906.10706](https://arxiv.org/abs/1906.10706)
8. P. Bergeron, S. Profumo, IceCube, DeepCore, PINGU and the indirect search for supersymmetric dark matter. JCAP **01**, 026 (2014). [arXiv:1312.4445](https://arxiv.org/abs/1312.4445)
9. M. van Beekveld, W. Beenakker, S. Caron, R. Peeters, R. Ruiz de Austri, Supersymmetry with Dark Matter is still natural. Phys. Rev. D **96**, 035015 (2017). [arXiv:1612.06333](https://arxiv.org/abs/1612.06333)
10. R.K. Barman, G. Belanger, B. Bhattacharjee, R. Godbole, G. Mendiratta, D. Sengupta, Invisible decay of the Higgs boson in the context of a thermal and nonthermal relic in MSSM. Phys. Rev. D **95**, 095018 (2017). [arXiv:1703.03838](https://arxiv.org/abs/1703.03838)
11. L. Roszkowski, E.M. Sessolo, S. Trojanowski, WIMP dark matter candidates and searches - current status and future prospects. Rep. Prog. Phys. **81**, 066201 (2018). [arXiv:1707.06277](https://arxiv.org/abs/1707.06277)
12. R. Kumar Barman, G. Bélanger, R.M. Godbole, Status of low mass LSP in SUSY. Eur. Phys. J. ST **229**, 3159–3185 (2020). [arXiv:2010.11674](https://arxiv.org/abs/2010.11674)
13. M. Van Beekveld, W. Beenakker, M. Schutten, J. De Wit, Dark matter, fine-tuning and  $(g-2)_\mu$  in the pMSSM. SciPost Phys. **11**, 049 (2021). [arXiv:2104.03245](https://arxiv.org/abs/2104.03245)
14. P. Fayet, Supergauge invariant extension of the Higgs mechanism and a model for the electron and its neutrino. Nucl. Phys. B **90**, 104–124 (1975)
15. J.R. Ellis, J. Gunion, H.E. Haber, L. Roszkowski, F. Zwirner, Higgs bosons in a nonminimal supersymmetric model. Phys. Rev. D **39**, 844 (1989)
16. L. Durand, J.L. Lopez, Upper bounds on Higgs and top quark masses in the flipped  $SU(5) \times U(1)$  superstring Model. Phys. Lett. B **217**, 463 (1989)
17. M. Drees, Supersymmetric models with extended Higgs sector. Int. J. Mod. Phys. A **4**, 3635 (1989)
18. U. Ellwanger, C. Hugonie, A.M. Teixeira, The next-to-minimal supersymmetric standard model. Phys. Rep. **496**, 1–77 (2010). [arXiv:0910.1785](https://arxiv.org/abs/0910.1785)

19. M. Maniatis, The next-to-minimal supersymmetric extension of the standard model reviewed. *Int. J. Mod. Phys. A* **25**, 3505–3602 (2010). [arXiv:0906.0777](#)
20. N.-E. Bomark, S. Moretti, S. Munir, L. Roszkowski, A light NMSSM pseudoscalar Higgs boson at the LHC redux. *JHEP* **02**, 044 (2015). [arXiv:1409.8393](#)
21. S. Ma, K. Wang, J. Zhu, Higgs decay to light (pseudo)scalars in the semi-constrained NMSSM. *Chin. Phys. C* **45**, 023113 (2021). [arXiv:2006.03527](#)
22. S.A. Abel, S. Sarkar, I.B. Whittingham, Neutralino dark matter in a class of unified theories. *Nucl. Phys. B* **392**, 83–110 (1993). [arXiv:hep-ph/9209292](#)
23. J. Kozaczuk, S. Profumo, Light NMSSM neutralino dark matter in the wake of CDMS II and a 126 GeV Higgs boson. *Phys. Rev. D* **89**, 095012 (2014). [arXiv:1308.5705](#)
24. J. Cao, C. Han, L. Wu, P. Wu, J.M. Yang, A light SUSY dark matter after CDMS-II, LUX and LHC Higgs data. *JHEP* **05**, 056 (2014). [arXiv:1311.0678](#)
25. T. Han, Z. Liu, S. Su, Light neutralino dark matter: direct/indirect detection and collider searches. *JHEP* **08**, 093 (2014). [arXiv:1406.1181](#)
26. U. Ellwanger, C. Hugonie, The semi-constrained NMSSM satisfying bounds from the LHC, LUX and Planck. *JHEP* **08**, 046 (2014). [arXiv:1405.6647](#)
27. R.K. Barman, G. Bélanger, B. Bhattacharjee, R. Godbole, D. Sengupta, X. Tata, Current bounds and future prospects of light neutralino dark matter in NMSSM. *Phys. Rev. D* **103**, 015029 (2021). [arXiv:2006.07854](#)
28. J.-J. Cao, K.-I. Hikasa, W. Wang, J.M. Yang, K.-I. Hikasa, W.-Y. Wang et al., Light dark matter in NMSSM and implication on Higgs phenomenology. *Phys. Lett. B* **703**, 292–297 (2011). [arXiv:1104.1754](#)
29. D. Das, U. Ellwanger, A.M. Teixeira, Modified signals for supersymmetry in the NMSSM with a Singlino-like LSP. *JHEP* **04**, 067 (2012). [arXiv:1202.5244](#)
30. U. Ellwanger, Testing the higgsino–singlino sector of the NMSSM with trileptons at the LHC. *JHEP* **11**, 108 (2013). [arXiv:1309.1665](#)
31. J.S. Kim, T.S. Ray, The higgsino–singlino world at the large hadron collider. *Eur. Phys. J. C* **75**, 40 (2015). [arXiv:1405.3700](#)
32. U. Ellwanger, A.M. Teixeira, NMSSM with a singlino LSP: possible challenges for searches for supersymmetry at the LHC. *JHEP* **10**, 113 (2014). [arXiv:1406.7221](#)
33. C. Han, D. Kim, S. Munir, M. Park,  $\mathcal{O}(1)$  GeV dark matter in SUSY and a very light pseudoscalar at the LHC. *JHEP* **07**, 002 (2015). [arXiv:1504.05085](#)
34. C.T. Potter, Natural NMSSM with a light singlet Higgs and singlino LSP. *Eur. Phys. J. C* **76**, 44 (2016). [arXiv:1505.05554](#)
35. R. Enberg, S. Munir, C. Pérez de los Heros, D. Werder, Prospects for higgsino–singlino dark matter detection at IceCube and PINGU. [arXiv:1506.05714](#)
36. U. Ellwanger, Present status and future tests of the higgsino–singlino sector in the NMSSM. *JHEP* **02**, 051 (2017). [arXiv:1612.06574](#)
37. G. Pozzo, Y. Zhang, Constraining resonant dark matter with combined LHC electroweak searches. *Phys. Lett. B* **789**, 582–591 (2019). [arXiv:1807.01476](#)
38. F. Domingo, J.S. Kim, V.M. Lozano, P. Martin-Ramiro, R. Ruiz de Austri, Confronting the neutralino and chargino sector of the NMSSM with the multilepton searches at the LHC. *Phys. Rev. D* **101**, 075010 (2020). [arXiv:1812.05186](#)
39. U. Ellwanger, C. Hugonie, The higgsino–singlino sector of the NMSSM: combined constraints from dark matter and the LHC. *Eur. Phys. J. C* **78**, 735 (2018). [arXiv:1806.09478](#)
40. W. Abdallah, A. Chatterjee, A. Datta, Revisiting singlino dark matter of the natural  $Z_3$ -symmetric NMSSM in the light of LHC. *JHEP* **09**, 095 (2019). [arXiv:1907.06270](#)
41. M. Guchait, A. Roy, Light singlino dark matter at the LHC. *Phys. Rev. D* **102**, 075023 (2020). [arXiv:2005.05190](#)
42. K. Wang, J. Zhu, Funnel annihilations of light dark matter and the invisible decay of the Higgs boson. *Phys. Rev. D* **101**, 095028 (2020). [arXiv:2003.01662](#)
43. F. Ferrer, L.M. Krauss, S. Profumo, Indirect detection of light neutralino dark matter in the NMSSM. *Phys. Rev. D* **74**, 115007 (2006). [arXiv:hep-ph/0609257](#)
44. S. Demidov, O. Suvorova, Annihilation of NMSSM neutralinos in the Sun and neutrino telescope limits. *JCAP* **06**, 018 (2010). [arXiv:1006.0872](#)
45. K. Wang, J. Zhu, Q. Jie, Higgsino asymmetry and direct-detection constraints of light dark matter in the NMSSM with non-universal Higgs masses. *Chin. Phys. C* **45**, 041003 (2021). [arXiv:2011.12848](#)
46. G. Beck, R. Temo, E. Malwa, M. Kumar, B. Mellado, Connecting multi-lepton anomalies at the LHC and in astrophysics with MeerKAT/SKA. [arXiv:2102.10596](#)
47. A. Sakharov, Violation of CP invariance, c asymmetry, and baryon asymmetry of the universe. *Pisma. Zh. Eksp. Teor. Fiz.* **5**, 32–35 (1967)
48. A.G. Cohen, D. Kaplan, A. Nelson, Progress in electroweak baryogenesis. *Annu. Rev. Nucl. Part. Sci.* **43**, 27–70 (1993). [arXiv:hep-ph/9302210](#)
49. M. Quiros, Field theory at finite temperature and phase transitions. *Helv. Phys. Acta* **67**, 451–583 (1994)
50. V. Rubakov, M. Shaposhnikov, Electroweak baryon number non-conservation in the early universe and in high-energy collisions. *Usp. Fiz. Nauk* **166**, 493–537 (1996). [arXiv:hep-ph/9603208](#)
51. M. Trodden, Electroweak baryogenesis. *Rev. Mod. Phys.* **71**, 1463–1500 (1999). [arXiv:hep-ph/9803479](#)
52. A. Pilaftsis, CP odd tadpole renormalization of Higgs scalar–pseudoscalar mixing. *Phys. Rev. D* **58**, 096010 (1998). [arXiv:hep-ph/9803297](#)
53. A. Pilaftsis, Higgs scalar–pseudoscalar mixing in the minimal supersymmetric standard model. *Phys. Lett. B* **435**, 88–100 (1998). [arXiv:hep-ph/9805373](#)
54. A. Pilaftsis, C.E. Wagner, Higgs bosons in the minimal supersymmetric standard model with explicit CP violation. *Nucl. Phys. B* **553**, 3–42 (1999). [arXiv:hep-ph/9902371](#)
55. M.S. Carena, J.R. Ellis, A. Pilaftsis, C. Wagner, Renormalization group improved effective potential for the MSSM Higgs sector with explicit CP violation. *Nucl. Phys. B* **586**, 92–140 (2000). [arXiv:hep-ph/0003180](#)
56. S. Choi, M. Drees, J.S. Lee, Loop corrections to the neutral Higgs boson sector of the MSSM with explicit CP violation. *Phys. Lett. B* **481**, 57–66 (2000). [arXiv:hep-ph/0002287](#)
57. M.S. Carena, J.R. Ellis, A. Pilaftsis, C. Wagner, Higgs boson pole masses in the MSSM with explicit CP violation. *Nucl. Phys. B* **625**, 345–371 (2002). [arXiv:hep-ph/0111245](#)
58. M.S. Carena, J.R. Ellis, S. Mrenna, A. Pilaftsis, C. Wagner, Collider probes of the MSSM Higgs sector with explicit CP violation. *Nucl. Phys. B* **659**, 145–178 (2003). [arXiv:hep-ph/0211467](#)
59. S. Choi, J. Kalinowski, Y. Liao, P. Zerwas, H/A Higgs mixing in CP-noninvariant supersymmetric theories. *Eur. Phys. J. C* **40**, 555–564 (2005). [arXiv:hep-ph/0407347](#)
60. M. Frank, T. Hahn, S. Heinemeyer, W. Hollik, H. Rzehak, G. Weiglein, The Higgs boson masses and mixings of the complex MSSM in the Feynman-diagrammatic approach. *JHEP* **02**, 047 (2007). [arXiv:hep-ph/0611326](#)
61. S. Heinemeyer, W. Hollik, H. Rzehak, G. Weiglein, The Higgs sector of the complex MSSM at two-loop order: QCD contributions. *Phys. Lett. B* **652**, 300–309 (2007). [arXiv:0705.0746](#)
62. M. Carena, J. Ellis, J.S. Lee, A. Pilaftsis, C.E.M. Wagner, CP violation in heavy MSSM Higgs scenarios. *JHEP* **02**, 123 (2016). [arXiv:1512.00437](#)

63. F. Mahmoudi, Supersymmetry, direct and indirect constraints. Nucl. Part. Phys. Proc. **303–305**, 37–42 (2018). [arXiv:1812.08783](#)
64. M.S. Carena, J.R. Ellis, A. Pilaftsis, C. Wagner, CP violating MSSM Higgs bosons in the light of LEP-2. Phys. Lett. B **495**, 155–163 (2000). [arXiv:hep-ph/0009212](#)
65. S. Abel, S. Khalil, O. Lebedev, EDM constraints in supersymmetric theories. Nucl. Phys. B **606**, 151–182 (2001). [arXiv:hep-ph/0103320](#)
66. M.D. Goodsell, F. Staub, The Higgs mass in the CP violating MSSM, NMSSM, and beyond. Eur. Phys. J. C **77**, 46 (2017). [arXiv:1604.05335](#)
67. R. Grober, M. Muhlleitner, M. Spira, Higgs pair production at NLO QCD for CP-violating Higgs sectors. Nucl. Phys. B **925**, 1–27 (2017). [arXiv:1705.05314](#)
68. T.N. Dao, R. Gröber, M. Krause, M. Muhlleitner, H. Rzehak, Two-loop  $\mathcal{O}(\alpha_t^2)$  corrections to the neutral Higgs boson masses in the CP-violating NMSSM. JHEP **08**, 114 (2019). [arXiv:1903.11358](#)
69. T.N. Dao, M. Muhlleitner, S. Patel, K. Sakurai, One-loop corrections to the two-body decays of the charged Higgs bosons in the real and complex NMSSM. Eur. Phys. J. C **81**, 340 (2021). [arXiv:2012.14889](#)
70. F. Domingo, S. Paßehr, Fighting off field dependence in MSSM Higgs-mass corrections of order  $\alpha_t \alpha_s$  and  $\alpha_t^2$ . Eur. Phys. J. C **81**, 661 (2021). [arXiv:2105.01139](#)
71. T.N. Dao, M. Gabelmann, M. Muhlleitner, H. Rzehak, Two-loop  $\mathcal{O}((t + \lambda + \kappa)^2)$  corrections to the Higgs boson masses in the CP-violating NMSSM. JHEP **09**, 193 (2021). [arXiv:2106.06990](#)
72. P. Slavich et al., Higgs-mass predictions in the MSSM and beyond. Eur. Phys. J. C **81**, 450 (2021). [arXiv:2012.15629](#)
73. T. Graf, R. Grober, M. Muhlleitner, H. Rzehak, K. Walz, Higgs boson masses in the complex NMSSM at one-loop level. JHEP **1210**, 122 (2012). [arXiv:1206.6806](#)
74. S. Moretti, S. Munir, P. Poulose, 125 GeV Higgs boson signal within the complex NMSSM. Phys. Rev. D **89**, 015022 (2014). [arXiv:1305.0166](#)
75. S. Munir, Novel Higgs-to-125 GeV Higgs boson decays in the complex NMSSM. Phys. Rev. D **89**, 095013 (2014). [arXiv:1310.8129](#)
76. S.F. King, M. Muhlleitner, R. Nevzorov, K. Walz, Exploring the CP-violating NMSSM: EDM constraints and phenomenology. Nucl. Phys. B **901**, 526–555 (2015). [arXiv:1508.03255](#)
77. S. Moretti, S. Munir, Two Higgs bosons near 125 GeV in the complex NMSSM and the LHC Run I data. Adv. High Energy Phys. **2015**, 509847 (2015). [arXiv:1505.00545](#)
78. B. Das, S. Moretti, S. Munir, P. Poulose, Two Higgs bosons near 125 GeV in the NMSSM: beyond the narrow width approximation. Eur. Phys. J. C **77**, 544 (2017). [arXiv:1704.02941](#)
79. F. Domingo, A new tool for the study of the CP-violating NMSSM. JHEP **06**, 052 (2015). [arXiv:1503.07087](#)
80. D.J. Miller, R. Nevzorov, P.M. Zerwas, The Higgs sector of the next-to-minimal supersymmetric standard model. Nucl. Phys. B **681**, 3–30 (2004). [arXiv:hep-ph/0304049](#)
81. ACME Collaboration, V. Andreev et al., Improved limit on the electric dipole moment of the electron. Nature **562**, 355–360 (2018)
82. nEDM Collaboration, C. Abel et al., Measurement of the permanent electric dipole moment of the neutron. Phys. Rev. Lett. **124**, 081803 (2020). [arXiv:2001.11966](#)
83. W.B. Cairncross, D.N. Gresh, M. Grau, K.C. Cossel, T.S. Roussy, Y. Ni et al., Precision measurement of the electron's electric dipole moment using trapped molecular ions. Phys. Rev. Lett. **119**, 153001 (2017). [arXiv:1704.07928](#)
84. W.C. Griffith, M.D. Swallows, T.H. Loftus, M.V. Romalis, B.R. Heckel, E.N. Fortson, Improved limit on the permanent electric dipole moment of Hg-199. Phys. Rev. Lett. **102**, 101601 (2009). [arXiv:0901.2328](#)
85. B.C. Regan, E.D. Commins, C.J. Schmidt, D. DeMille, New limit on the electron electric dipole moment. Phys. Rev. Lett. **88**, 071805 (2002)
86. K. Cheung, T.-J. Hou, J.S. Lee, E. Senaha, The Higgs boson sector of the next-to-MSSM with CP violation. Phys. Rev. D **82**, 075007 (2010). [arXiv:1006.1458](#)
87. K. Cheung, T.-J. Hou, J.S. Lee, E. Senaha, Higgs mediated EDMs in the next-to-MSSM: an application to electroweak baryogenesis. Phys. Rev. D **84**, 015002 (2011). [arXiv:1102.5679](#)
88. W. Porod, SPheno, a program for calculating supersymmetric spectra, SUSY particle decays and SUSY particle production at  $e^+e^-$  colliders. Comput. Phys. Commun. **153**, 275–315 (2003). [arXiv:hep-ph/0301101](#)
89. W. Porod, F. Staub, SPheno 3.1: extensions including flavour, CP-phases and models beyond the MSSM. Comput. Phys. Commun. **183**, 2458–2469 (2012). [arXiv:1104.1573](#)
90. F. Staub, SARAH. [arXiv:0806.0538](#)
91. F. Staub, SARAH 4: a tool for (not only SUSY) model builders. Comput. Phys. Commun. **185**, 1773–1790 (2014). [arXiv:1309.7223](#)
92. M.D. Goodsell, K. Nickel, F. Staub, Two-loop Higgs mass calculations in supersymmetric models beyond the MSSM with SARAH and SPheno. Eur. Phys. J. C **75**, 32 (2015). [arXiv:1411.0675](#)
93. M. Goodsell, K. Nickel, F. Staub, Generic two-loop Higgs mass calculation from a diagrammatic approach. Eur. Phys. J. C **75**, 290 (2015). [arXiv:1503.03098](#)
94. F. Staub, Exploring new models in all detail with SARAH. Adv. High Energy Phys. **2015**, 840780 (2015). [arXiv:1503.04200](#)
95. J. Braathen, M.D. Goodsell, F. Staub, Supersymmetric and non-supersymmetric models without catastrophic Goldstone bosons. Eur. Phys. J. C **77**, 757 (2017). [arXiv:1706.05372](#)
96. J. Baglio, R. Gröber, M. Muhlleitner, D. Nhung, H. Rzehak, M. Spira et al., NMSSMCALC: a program package for the calculation of loop-corrected Higgs boson masses and decay widths in the (complex) NMSSM. Comput. Phys. Commun. **185**, 3372–3391 (2014). [arXiv:1312.4788](#)
97. M.D. Goodsell, S. Liebler, F. Staub, Generic calculation of two-body partial decay widths at the full one-loop level. Eur. Phys. J. C **77**, 758 (2017). [arXiv:1703.09237](#)
98. F. Feroz, M. Hobson, M. Bridges, MultiNest: an efficient and robust Bayesian inference tool for cosmology and particle physics. Mon. Not. R. Astron. Soc. **398**, 1601–1614 (2009). [arXiv:0809.3437](#)
99. A. Belyaev, N.D. Christensen, A. Pukhov, CalcHEP 3.4 for collider physics within and beyond the Standard Model. Comput. Phys. Commun. **184**, 1729–1769 (2013). [arXiv:1207.6082](#)
100. G. Belanger, F. Boudjema, A. Pukhov, A. Semenov, MicrOMEGAs 2.0: a program to calculate the relic density of dark matter in a generic model. Comput. Phys. Commun. **176**, 367–382 (2007). [arXiv:hep-ph/0607059](#)
101. G. Bélanger, F. Boudjema, A. Pukhov, A. Semenov, MicrOMEGAs4.1: two dark matter candidates. Comput. Phys. Commun. **192**, 322–329 (2015). [arXiv:1407.6129](#)
102. D. Barducci, G. Belanger, J. Bernon, F. Boudjema, J. Da Silva, S. Kraml et al., Collider limits on new physics within micrOMEGAs\_4.3. Comput. Phys. Commun. **222**, 327–338 (2018). [arXiv:1606.03834](#)
103. ATLAS, CMS Collaborations, J.M. Langford, Combination of Higgs measurements from ATLAS and CMS: couplings and  $\kappa$ -framework. PoS LHCP2020, 136 (2021)
104. P. Bechtle, S. Heinemeyer, T. Klingl, T. Stefaniak, G. Weiglein, J. Wittbrodt, HiggsSignals-2: probing new physics with precision Higgs measurements in the LHC 13 TeV era. [arXiv:2012.09197](#)
105. HFLAV Collaboration, Y. Amhis et al., Averages of  $b$ -hadron,  $c$ -hadron, and  $\tau$ -lepton properties as of summer 2016. Eur. Phys. J. C **77**, 895 (2017). [arXiv:1612.07233](#)



106. LHCb Collaboration, R. Aaij et al., Measurement of the  $B_s^0 \rightarrow \mu^+ \mu^-$  branching fraction and effective lifetime and search for  $B^0 \rightarrow \mu^+ \mu^-$  decays. *Phys. Rev. Lett.* **118**, 191801 (2017). [arXiv:1703.05747](#)
107. P. Bechtle, D. Dercks, S. Heinemeyer, T. Klingl, T. Stefaniak, G. Weiglein et al., HiggsBounds-5: testing Higgs sectors in the LHC 13 TeV Era. *Eur. Phys. J. C* **80**, 1211 (2020). [arXiv:2006.06007](#)
108. Planck Collaboration, N. Aghanim et al., Planck 2018 results. VI. Cosmological parameters. *Astron. Astrophys.* **641**, A6 (2020). [arXiv:1807.06209](#)
109. N. Baro, F. Boudjema, A. Semenov, Full one-loop corrections to the relic density in the MSSM: a few examples. *Phys. Lett. B* **660**, 550–560 (2008). [arXiv:0710.1821](#)
110. F. Boudjema, G. Drieu La Rochelle, S. Kulkarni, One-loop corrections, uncertainties and approximations in neutralino annihilations: examples. *Phys. Rev. D* **84**, 116001 (2011). [arXiv:1108.4291](#)
111. M. Beneke, F. Dighera, A. Hryczuk, Relic density computations at NLO: infrared finiteness and thermal correction. *JHEP* **10**, 045 (2014). [arXiv:1409.3049](#)
112. G. Belanger, V. Bizouard, F. Boudjema, G. Chalons, One-loop renormalization of the NMSSM in SloopS: The neutralino-chargino and sfermion sectors. *Phys. Rev. D* **93**, 115031 (2016). [arXiv:1602.05495](#)
113. J. Harz, B. Herrmann, M. Klasen, K. Kovarik, P. Steppeler, Theoretical uncertainty of the supersymmetric dark matter relic density from scheme and scale variations. *Phys. Rev. D* **93**, 114023 (2016). [arXiv:1602.08103](#)
114. S. Schmiemann, J. Harz, B. Herrmann, M. Klasen, K. Kovařík, Squark-pair annihilation into quarks at next-to-leading order. *Phys. Rev. D* **99**, 095015 (2019). [arXiv:1903.10998](#)
115. J. Branahl, J. Harz, B. Herrmann, M. Klasen, K. Kovařík, S. Schmiemann, SUSY-QCD corrected and Sommerfeld enhanced stau annihilation into heavy quarks with scheme and scale uncertainties. *Phys. Rev. D* **100**, 115003 (2019). [arXiv:1909.09527](#)
116. B.S. Acharya, P. Kumar, K. Bobkov, G. Kane, J. Shao, S. Watson, Non-thermal dark matter and the moduli problem in string frameworks. *JHEP* **06**, 064 (2008). [arXiv:0804.0863](#)
117. K.M. Zurek, Multi-component dark matter. *Phys. Rev. D* **79**, 115002 (2009). [arXiv:0811.4429](#)
118. PandaX-4T Collaboration, Y. Meng et al., Dark matter search results from the PandaX-4T commissioning run. *Phys. Rev. Lett.* **127**, 261802 (2021). [arXiv:2107.13438](#)
119. XENON Collaboration, E. Aprile et al., Dark matter search results from a one ton-year exposure of XENON1T. *Phys. Rev. Lett.* **121**, 111302 (2018). [arXiv:1805.12562](#)
120. ATLAS Collaboration, G. Aad et al., Search for invisible Higgs-boson decays in events with vector-boson fusion signatures using 139 fb<sup>-1</sup> of proton–proton data recorded by the ATLAS experiment. [arXiv:2202.07953](#)
121. CMS Collaboration, A. Tumasyan et al., Search for invisible decays of the Higgs boson produced via vector boson fusion in proton-proton collisions at  $\sqrt{s} = 13$  TeV. [arXiv:2201.11585](#)
122. ATLAS Collaboration, G. Aad et al., Search for electroweak production of charginos and sleptons decaying into final states with two leptons and missing transverse momentum in  $\sqrt{s} = 13$  TeV  $pp$  collisions using the ATLAS detector. *Eur. Phys. J. C* **80**, 123 (2020). [arXiv:1908.08215](#)
123. ATLAS Collaboration, G. Aad et al., Search for direct production of electroweakinos in final states with one lepton, missing transverse momentum and a Higgs boson decaying into two  $b$ -jets in  $pp$  collisions at  $\sqrt{s} = 13$  TeV with the ATLAS detector. *Eur. Phys. J. C* **80**, 691 (2020). [arXiv:1909.09226](#)
124. ATLAS Collaboration, G. Aad et al., Search for chargino-neutralino production with mass splittings near the electroweak scale in three-lepton final states in  $\sqrt{s}=13$  TeV  $pp$  collisions with the ATLAS detector. *Phys. Rev. D* **101**, 072001 (2020). [arXiv:1912.08479](#)
125. ATLAS Collaboration, G. Aad et al., Search for chargino-neutralino pair production in final states with three leptons and missing transverse momentum in  $\sqrt{s} = 13$  TeV  $pp$  collisions with the ATLAS detector. *Eur. Phys. J. C* **81**, 1118 (2021). [arXiv:2106.01676](#)
126. S. Kraml, S. Kulkarni, U. Laa, A. Lessa, W. Magerl, D. Proschofsky-Spindler et al., SModelS: a tool for interpreting simplified-model results from the LHC and its application to supersymmetry. *Eur. Phys. J. C* **74**, 2868 (2014). [arXiv:1312.4175](#)
127. F. Ambrogio, S. Kraml, S. Kulkarni, U. Laa, A. Lessa, SModelS v1.1 user manual: improving simplified model constraints with efficiency maps. *Comput. Phys. Commun.* **227**, 72–98 (2018). [arXiv:1701.06586](#)
128. F. Ambrogio et al., SModelS v1.2: long-lived particles, combination of signal regions, and other novelties. *Comput. Phys. Commun.* **251**, 106848 (2020). [arXiv:1811.10624](#)
129. C.K. Khosa, S. Kraml, A. Lessa, P. Neuhuber, W. Waltenberger, SModelS database update v1.2.3. *LHEP* **2020**, 158 (2020)
130. G. Alguero, J. Heisig, C. Khosa, S. Kraml, S. Kulkarni, A. Lessa et al., Constraining new physics with SModelS version 2. [arXiv:2112.00769](#)
131. E. Conte, B. Fuks, G. Serret, MadAnalysis 5, a user-friendly framework for collider phenomenology. *Comput. Phys. Commun.* **184**, 222–256 (2013). [arXiv:1206.1599](#)
132. E. Conte, B. Dumont, B. Fuks, C. Wymant, Designing and recasting LHC analyses with MadAnalysis 5. *Eur. Phys. J. C* **74**, 3103 (2014). [arXiv:1405.3982](#)
133. B. Dumont, B. Fuks, S. Kraml, S. Bein, G. Chalons, E. Conte et al., Toward a public analysis database for LHC new physics searches using MADANALYSIS 5. *Eur. Phys. J. C* **75**, 56 (2015). [arXiv:1407.3278](#)
134. E. Conte, B. Fuks, Confronting new physics theories to LHC data with MADANALYSIS 5. *Int. J. Mod. Phys. A* **33**, 1830027 (2018). [arXiv:1808.00480](#)
135. M.D. Goodsell, Implementation of the ATLAS-SUSY-2019-08 analysis in the MadAnalysis 5 framework (electroweakinos with a Higgs decay into a  $b\bar{b}$  pair, one lepton and missing transverse energy; 139/fb). *Mod. Phys. Lett. A* **36**, 2141006 (2021)
136. B. Fuks et al., Proceedings of the second MadAnalysis 5 workshop on LHC recasting in Korea. *Mod. Phys. Lett. A* **36**, 2102001 (2021). [arXiv:2101.02245](#)
137. LHC Reinterpretation Forum Collaboration, W. Abdallah et al., *Reinterpretation of LHC results for new physics: status and recommendations after Run 2*. *SciPost Phys.* **9**, 022 (2020). [arXiv:2003.07868](#)
138. M.D. Goodsell, S. Kraml, H. Reyes-González, S.L. Williamson, Constraining electroweakinos in the minimal dirac gaugino model. *SciPost Phys.* **9**, 047 (2020). [arXiv:2007.08498](#)